AIMS Mathematics, 11(5): 14870–14914.
DOI: 10.3934/math.2026613
Received: 13 January 2026
Revised: 26 April 2026
Accepted: 11 May 2026
Published: 27 May 2026

http://www.aimspress.com/journal/Math

Research article

A new extended distribution with monotonic and nonmonotonic failure rates: statistical properties and comparative predictive modeling in medical datasets

Abdulrahman M. A. Aldawsari[1,*], Zahrah Fayez Althobaiti[2], Aminu Suleiman Mohammed[3] and Abdulmajeed A. R. Alharbi[4]

[1] Department of Mathematics, College of Sciences and Humanities, Prince Sattam Bin Abdulaziz University, Al-Kharj 16273, Saudi Arabia

[2] Department of Statistics, Faculty of Science, University of Tabuk, Tabuk 71491, Saudi Arabia

[3] Department of Statistics, Ahmadu Bello University, Zaria, Nigeria

[4] Department of Statistics and Operations Research, College of Science, King Saud University, P.O. Box 2455, Riyadh 11451, Saudi Arabia

* **Correspondence:** Email: abd.aldawsari@psau.edu.sa.

Abstract: This study introduces a new continuous probability distribution, termed the extended bounded sine hyperbolic (EBSH) distribution, for modeling non-negative data with flexible structural properties. The distribution accommodates symmetric and skewed behaviors and captures a wide range of hazard rate patterns, including increasing, decreasing, and bathtub-shaped forms. Beyond its theoretical contribution, the study investigates the use of the EBSH distribution as a feature engineering mechanism in machine learning. Raw input variables are transformed through the EBSH formulation to enhance data representation and improve predictive performance. The approach is evaluated using COVID-19 mortality and breast cancer datasets, using models such as recurrent neural networks (RNN) and support vector regression (SVR). Experimental results indicate that EBSH-based feature engineering improves prediction accuracy compared to raw features. For the COVID-19 dataset, the RNN model achieved a mean absolute error (MAE) of 0.0296 and a root mean square error (RMSE) of 0.0373 using raw features, which further reduced to approximately 0.0251 (MAE) and 0.0328 (RMSE) after applying EBSH-based transformations. Similarly, for the breast cancer dataset, SVR produced an MAE of 4.0177 and an RMSE of 4.9926 with raw features, improving to about 3.6842 and 4.5213, respectively, under the engineered feature space. These findings demonstrate that the proposed EBSH distribution not only provides a flexible statistical modeling approach but also serves as an effective feature engineering tool that enhances machine learning performance across real-world datasets.

Keywords: survival function; medical data; extended bounded sine hyperbolic distribution; moments; parameter estimation
Mathematics Subject Classification: 62F10, 60E05, 62H12

1. Introduction

By utilizing the advantages of distinct algorithms and models, combining diverse artificial intelligence (AI) approaches can result in more accurate predictions [1, 2]. This method makes it possible to analyze data more thoroughly, which produces forecasts that are more solid and trustworthy [3]. Organizations can use AI's predictive capabilities while retaining a thorough understanding of the underlying processes by combining them with other techniques, such as conventional statistical models. Organizations can access a multitude of predictive power and improve their decision-making by carefully integrating AI technology with other approaches [4]. For example, AI is being utilized to detect risk factors, forecast patient outcomes, and customize treatment plans, often in conjunction with patient-specific data such as medical history. Data analysis, statistical modeling, and machine learning are used in AI predictive analytics in healthcare to foresee future health patterns and outcomes. This allows for preemptive treatments, which in turn enhances patient care. Good results and lower costs are eventually achieved by identifying high-risk individuals, forecasting the course of the disease, and customizing treatment regimens.

Numerous researchers have used AI to improve the prediction accuracies in many fields, such as the authors of [5], who studied the predictive mechanism of some AI methods in disease diagnosis. Saravi et al. [6] used AI methods in modeling and deciding on spine surgery, and Ghorbani et al. [7] studied multiple models using artificial intelligence in improving prediction accuracies using time series of river flow. Nia [8] used algorithms and an appropriate combination of AI for improving predictive accuracy management.

Numerous nations, many of which have started large immunization efforts, have authorized and delivered a number of COVID-19 vaccines. Physical or social separation, quarantining, ventilation of indoor areas, wearing face masks or other covers in public, covering coughs and sneezes, hand washing, and avoiding touching the face with dirty hands are further preventive methods. Although medications have been created to block the virus, supportive care, isolation, and experimental methods are still used to manage the illness, which is still primarily symptomatic. Toward the end of 2019, the World Health Organization (WHO) received reports of pneumonia cases in Wuhan, China, that had no recognized etiology. This was the first official case of COVID-19. Chinese authorities discovered a new coronavirus, temporarily known as 2019-nCoV, as the cause of these infections on January 7. Strict precautions were implemented globally to combat the pandemic. In March, travel bans and social distancing policies went into effect, along with recommendations for good handwashing practices. However, scientists realized that in order to combat the pandemic, a vaccine had to be created. On March 17, 2020, the first COVID-19 human vaccine trials began with the modern mRNA vaccine. These actions were only expected to limit the dissemination of the virus. Statistical models are extremely important in numerous areas. The goal of their creation was to deal with the pandemic. Models designed to fight various kinds of outbreaks are called epidemiological models. Mathematical

modeling is crucial for enhancing knowledge of disease dynamics and creating plans to stop the quick spread of illnesses in the lack of an appropriate vaccine or tailored antivirals. Numerous mathematical models have been proposed by researchers to evaluate the changing patterns and transmission of specific diseases, which may aid in the management of illness or even in the forecasting of future events [9].

When aberrant breast cells proliferate uncontrollably and develop tumors, it is known as breast cancer. Tumors can grow throughout the body and become lethal if left untreated. The milk ducts and/or the breast's milk-producing lobules are where breast cancer cells first appear. Early detection of the earliest form (in situ) is possible, and it poses little hazard to life. Cancer cells can invade neighboring breast tissue. This results in tumors that thicken or form lumps. According to human development, figures from throughout the world show startling disparities in the prevalence of breast cancer. For example, 1 in 12 women will receive a breast cancer diagnosis at some point in their lives, and 1 in 71 women will die from the disease in nations with extremely high Human Development Indexes (HDI). The majority of women who are diagnosed with breast cancer lack a known family history of the disease, even though a family history of the illness raises the likelihood of breast cancer. Nonetheless, a woman is not always at lower risk if there is no known family history [10].

Academic researchers have been working nonstop for years to develop a wide range of unique distributions tailored for particular practical uses. The core premise is that, as seen in fields such as ecology, hydrology, engineering, and drug development, among others, standard distributions typically fail to accurately represent reality. Creating suitable statistical models that can manage complicated real-world data is the aim of creating new distributions or enhancements. This flexibility can be attained by expanding conventional distribution's capacity to handle complex situations by incorporating new components [11].

The beta distribution is the statistical distribution that is most frequently used to represent data sets on the (0,1) interval [12]. In many statistical situations, it is a useful and practical model. Because of certain of its limitations, its ability to model data may not be sufficient to adequately explain the data. The lack of a closed form for its cumulative distribution function (CDF) is the beta distribution's main drawback. The Kumaraswamy distribution is a different widely used distribution that depends on unit spacing [13]. Although the Kumaraswamy distribution has a closed-form CDF, a significant disadvantage is that its moments do not have a closed-form solution. As a result, the literature has defined and used alternative distributions to the previously listed distributions. The logit slash [14], standard two-sided power [15], systems of frequency curves produced by methods of translation [16], Topp-Leone [17], exponentiated Topp-Leone [18], bounded exponentiated Lomax [19], bounded Burr XII [20], bounded gamma [21], bounded-exponentiated half-logistic [22], extended Topp-Leone [23], bounded power Lomax [24], unit (bounded) inverse exponentiated Weibull [25], and bounded sine hyperbolic (BSH) [26] distributions are a few examples. Some families of distributions involving the unit bound distributions, include the exponentiated-G, which was developed by using a uniform distribution [27], beta-G [28], Kumaraswamy-G [29], Topp-Leone Weibull-G [30], Topp-Leonne-G [31], and another new truncated generalized family [32].

Saeed et al. [26] developed the BSH distribution, which is more flexible than certain existing bounded distributions in the literature. The distribution may not be suitable in situations where significant outliers may arise or must be modeled, though, because it does not allow values outside of its designated limit. According to [18], the CDF and probability density function (PDF) of the

bounded sine hyperbolic distribution are as follows:

$$F(t) = \operatorname{csch}\left(\frac{\pi}{2}\right)\sinh\left(\frac{\pi}{2}t^{\theta}\right), \quad \theta > 0, \quad 0 < t < 1, \tag{1.1}$$

and

$$f(t) = \frac{\pi\theta}{2}\operatorname{csch}\left(\frac{\pi}{2}\right)t^{\theta-1}\cosh\left(\frac{\pi}{2}t^{\theta}\right), \quad \theta > 0, \quad 0 < t < 1, \tag{1.2}$$

where θ is a shape parameter.

A number of researchers in the statistical literature have concentrated on creating new and more adaptable statistical distributions by the application of appropriate transformation techniques [33–35]. Continuous random variables with boundless support are the subject of the majority of the derived distributions. The motivation of this research is to introduce a new open interval distribution using a transformation technique.

Despite the growing number of generalized and extended distributions in the literature, many existing models remain limited in their ability to capture diverse hazard rate behaviors and varying skewness structures. In particular, classical bounded distributions are often inadequate when modeling real-world phenomena that exhibit both monotonic and nonmonotonic failure rates alongside asymmetric patterns. This gap motivates the development of more flexible models that can accommodate complex data structures while maintaining analytical tractability. The proposed distribution in this study addresses these limitations by introducing additional flexibility through parameterization, enabling it to model a wider range of practical scenarios more effectively than existing alternatives.

This paper's main objective is to present a more adaptable distribution called extended bounded sine hyperbolic (EBSH) distribution based on the parameter induction approach. It is envisaged that this distribution will fit better than other lifespan distributions in some real-world situations. We are also driven by the growing significance of AI in predictive modeling as well as the necessity of reliable and flexible algorithms in the analysis of COVID-19 and breast cancer data. The statistical methodology considered in this study provides a flexible framework without introducing excessive complexity. This study expands the usefulness and adaptability of the conventional bounded sine hyperbolic (BSH) model. This paper derives several significant statistical features for the suggested distribution.

The key contributions of this study are summarized as follows:

i. To increase the classical BSH distribution's adaptability in simulating various events, the EBSH model shows hazard rates that are decreasing, J-shaped, and U-shaped. As a result, when the BSH model is not practically applicable, the EBSH model can be helpful.
ii. Among the key statistical characteristics that are obtained for the EBSH distribution are the analytical moment's expression, failure rate, quantile function, and linear representations.
iii. AI models for comparative prediction of COVID-19 and cancer, showcase the AI's potential in modern predictive analytics.
iv. The maximum likelihood estimation process evaluates the new distribution's inferential characteristics and creates a thorough framework for practitioners in the fields of AI and statistical modeling.
v. Offered practical distribution with uses in medicine, banking, engineering, and other domains for modeling asymmetric data, which is challenging for existing distributions and prediction algorithms to manage effectively.

This research can be organized as follows: The EBSH distribution's PDF, CDF, survival, hazard, mixing, and quantile functions are given in Section 2. Section 3 presents structural features of the EBSH distribution, such as linear representations, quantile functions, moments, and probability weighted moments. The maximum likelihood estimation is provided in Section 4. The model parameters are assessed through a simulation study utilizing various estimations approaches presented in Section 5. The adaptability of the novel distribution described in Section 6 are evaluated through applications to real-world datasets. In Section 7, prediction methodology using machine learning is discussed, and Section 8 provides conclusory remarks.

2. Developing extended bounded sine hyperbolic distribution

This section introduces a novel continuous probability distribution derived from the bounded sine hyperbolic distribution using a transformation strategy to study a new EBSH distribution. The transformation is based on the logarithmic technique with an extra shape parameter, as stated in

$$x^{\alpha} = -\log(1-t), \quad \text{which implies} \quad \frac{dt}{dx} = \alpha x^{\alpha-1} e^{-x^{\alpha}}. \tag{2.1}$$

Equations (1.2) and (2.1) are formulated as follows to yield the proposed EBSH distribution:

$$\begin{aligned} f(x) &= f(t)\left|\frac{dt}{dx}\right| \\ &= \frac{\pi\theta}{2}\operatorname{csch}\left(\frac{\pi}{2}\right)\left(1-e^{-x^{\alpha}}\right)^{\theta-1}\cosh\left\{\frac{\pi}{2}\left(1-e^{-x^{\alpha}}\right)^{\theta}\right\}\times\alpha x^{\alpha-1}e^{-x^{\alpha}} \\ &= \frac{\pi\alpha\theta}{2}\operatorname{csch}\left(\frac{\pi}{2}\right)x^{\alpha-1}e^{-x^{\alpha}}\left(1-e^{-x^{\alpha}}\right)^{\theta-1}\cosh\left\{\frac{\pi}{2}\left(1-e^{-x^{\alpha}}\right)^{\theta}\right\}, \quad \theta,\alpha>0, \;\; x>0, \end{aligned} \tag{2.2}$$

where θ and α are the shape parameters. The CDF of the EBSH distribution can be determined by integrating Eq (2.2) with respect to x as follows:

$$F(x) = \frac{\pi\alpha\theta}{2}\operatorname{csch}\left(\frac{\pi}{2}\right)\int_0^x y^{\alpha-1}e^{-y^{\alpha}}\left(1-e^{-y^{\alpha}}\right)^{\theta-1}\cosh\left\{\frac{\pi}{2}\left(1-e^{-y^{\alpha}}\right)^{\theta}\right\}dy. \tag{2.3}$$

Let

$$w_1 = 1-e^{-y^{\alpha}}, \quad \text{which implies} \quad dy = \frac{dw_1}{\alpha y^{\alpha-1}e^{-y^{\alpha}}}. \tag{2.4}$$

Substituting Eq (2.4) into Eq (2.3) produces the following result:

$$F(x) = \frac{\pi\theta}{2}\operatorname{csch}\left(\frac{\pi}{2}\right)\int_0^{1-e^{-x^{\alpha}}} w_1^{\theta-1}\cosh\left\{\frac{\pi}{2}w_1^{\theta}\right\}dw_1. \tag{2.5}$$

Let us define

$$w_2 = \frac{\pi}{2}w_1^{\theta}, \quad \text{which implies} \quad dw_1 = \frac{2}{\theta\pi w_1^{\theta-1}}dw_2. \tag{2.6}$$

Substituting Eq (2.6) into Eq (2.5) gives

$$
\begin{aligned}
F(x) &= \operatorname{csch}\left(\frac{\pi}{2}\right) \int_0^{\frac{\pi}{2}\left(1-e^{-x^{\alpha}}\right)^{\theta}} \cosh(w_2)dw_2 \\
&= \operatorname{csch}\left(\frac{\pi}{2}\right)(\sinh(w_2)]_0^{\frac{\pi}{2}\left(1-e^{-x^{\alpha}}\right)^{\theta}} \\
&= \operatorname{csch}\left(\frac{\pi}{2}\right)\left\{\sinh\left(\frac{\pi}{2}\left(1-e^{-x^{\alpha}}\right)^{\theta}\right)-\sinh(0)\right\} \\
&= \operatorname{csch}\left(\frac{\pi}{2}\right)\left\{\sinh\left(\frac{\pi}{2}\left(1-e^{-x^{\alpha}}\right)^{\theta}\right)\right\}, \quad \theta,\alpha>0, \quad x>0. \qquad (2.7)
\end{aligned}
$$

The visual structure of the PDF of the EBSH distribution will be addressed in this section. Figure 1 shows the PDF of the new model with different combinations of parameters. The PDF in Figure 1 exhibits a variety of features, such as (a) right-skewed, (b) left-skewed, and (c) near-symmetry. This illustrates how the model may capture a variety of distribution shapes. These forms represent many situations that occur in the actual world. For instance, a left-skewed PDF can model datasets with longer survival times for the majority of patients, but a right-skewed PDF can depict survival times where most patients have shorter durations. It is crucial to recognize the limitations of the EBSH model when modeling datasets with multimodal patterns, even if it is excellent at capturing a wide range of distribution forms.

Table 1 displays the EBSH distribution's PDF values for random variable values ranging from 0.1 to 4 and θ parameter values between 0.5 and 3. Following the development of an algorithm for the density of the EBSH distribution, the numbers in the table were obtained using R software. The table shows that the values for the EBSH distribution's PDF decrease as x increases. This suggests that the EBSH distribution's PDF has a right-skewed structure. When $\alpha = 0.5$, it was observed that across all the values of x, the values of the PDF decrease with an increase in the value of the parameter θ.

Table 2 displays the EBSH distribution's PDF values for random variable values ranging from 0.1 to 4 and θ parameter values between 0.5 and 3. Following the development of an algorithm for the density of the EBSH distribution, the outcomes in the table were obtained using R software. The table shows that the values for the EBSH distribution's PDF decrease as x increases when taking the least values of $\theta = 0.5$ and 1. This suggests that the EBSH distribution's PDF has a right-skewed structure. For $\theta = 1.5$, the values start rising as the random variable increased, and at some point they fall. This signifies that the PDF has a unimodal structure and can be used to model data with a positive direction. When $\theta = 2, 2.5$, and 3, it is observed that the values of the PDF increase with an increase in the value of the random variable. This means that the PDF has a left-skewed structure and can be used to model data that is negatively skewed.

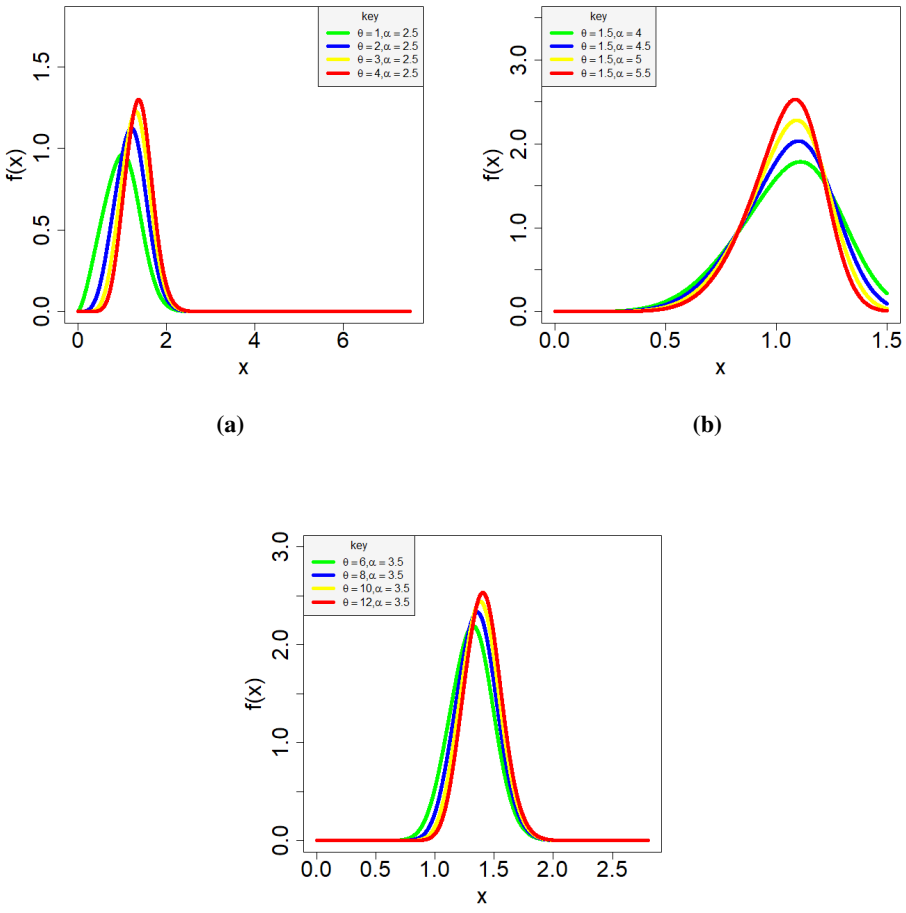

Figure 1. The PDF plot of the EBSH distribution.

Table 3 displays the EBSH distribution's PDF values for random variable values ranging from 0.1 to 4 and α parameter values between 0.2 and 1.2. Following the development of an algorithm for the density of the EBSH distribution, the results in the table were obtained using the R software. The table shows that the values for the EBSH distribution's PDF decrease as the random variable increases. This shows that the PDF has a right-skewed structure and is capable of modeling right-skewed data sets.

Table 4 displays the EBSH distribution's PDF values for random variable values ranging from 0.1 to 4 and α parameter values between 0.2 and 1.2. Following the development of an algorithm for the density of the EBSH distribution, the results in the table were obtained using the R software. The table shows that the values for the EBSH distribution's PDF decrease as the random variable increases, except when $\alpha = 1.2$. This shows that the PDF has a right-skewed structure and is capable of modeling right-skewed data sets. For $\alpha = 1.2$, the values of the PDF increase and decrease at some point, meaning the PDF has a unimodal shape.

Table 1. Statistical table for the probability density function of the EBSH distribution when $\alpha = 0.5$.

x	$\theta = 0.5$	$\theta = 1$	$\theta = 1.5$	$\theta = 2$	$\theta = 2.5$	$\theta = 3$
0.1	1.0225	0.8591	0.6296	0.4294	0.2781	0.1735
0.2	0.6008	0.5683	0.4652	0.3593	0.2661	0.1909
0.3	0.4347	0.4423	0.384	0.3159	0.2508	0.1936
0.4	0.3426	0.368	0.3326	0.2849	0.2364	0.1914
0.5	0.283	0.3175	0.2961	0.2612	0.2237	0.1873
0.6	0.2409	0.2803	0.2683	0.2422	0.2123	0.1824
0.7	0.2094	0.2515	0.2461	0.2264	0.2023	0.1773
0.8	0.1849	0.2282	0.2278	0.2129	0.1933	0.1722
0.9	0.1652	0.209	0.2122	0.2013	0.1852	0.1673
1	0.149	0.1927	0.1989	0.191	0.1778	0.1625
1.1	0.1354	0.1787	0.1871	0.1819	0.1711	0.1579
1.2	0.1239	0.1665	0.1768	0.1736	0.1648	0.1536
1.3	0.1139	0.1558	0.1674	0.1662	0.1591	0.1494
1.4	0.1053	0.1462	0.159	0.1593	0.1538	0.1455
1.5	0.0977	0.1376	0.1514	0.153	0.1488	0.1417
1.6	0.091	0.1299	0.1444	0.1471	0.1441	0.1381
1.7	0.085	0.1229	0.1379	0.1417	0.1396	0.1347
1.8	0.0796	0.1165	0.132	0.1366	0.1355	0.1314
1.9	0.0748	0.1106	0.1265	0.1318	0.1315	0.1282
2	0.0704	0.1053	0.1213	0.1273	0.1277	0.1251
2.1	0.0664	0.1003	0.1165	0.123	0.1241	0.1222
2.2	0.0628	0.0957	0.112	0.119	0.1207	0.1194
2.3	0.0595	0.0914	0.1077	0.1152	0.1174	0.1166
2.4	0.0564	0.0874	0.1038	0.1116	0.1143	0.114
2.5	0.0536	0.0837	0.1	0.1081	0.1113	0.1114
2.6	0.051	0.0802	0.0965	0.1048	0.1084	0.109
2.7	0.0486	0.077	0.0931	0.1017	0.1056	0.1066
2.8	0.0463	0.0739	0.0899	0.0987	0.1029	0.1043
2.9	0.0442	0.071	0.0869	0.0958	0.1003	0.102
3	0.0423	0.0683	0.084	0.0931	0.0978	0.0998
3.1	0.0404	0.0657	0.0813	0.0904	0.0954	0.0977
3.2	0.0387	0.0633	0.0786	0.0879	0.0931	0.0956
3.3	0.0371	0.061	0.0762	0.0855	0.0909	0.0936
3.4	0.0356	0.0588	0.0738	0.0831	0.0887	0.0916
3.5	0.0342	0.0568	0.0715	0.0809	0.0866	0.0897
3.6	0.0328	0.0548	0.0693	0.0787	0.0845	0.0879
3.7	0.0316	0.0529	0.0672	0.0766	0.0825	0.086
3.8	0.0304	0.0512	0.0653	0.0746	0.0806	0.0843
3.9	0.0293	0.0495	0.0633	0.0727	0.0788	0.0826
4	0.0282	0.0479	0.0615	0.0708	0.077	0.0809

Table 2. Statistical table for the probability density function of the EBSH distribution when $\alpha = 1$.

x	$\theta = 0.5$	$\theta = 1$	$\theta = 1.5$	$\theta = 2$	$\theta = 2.5$	$\theta = 3$
0.1	1.1209	0.6245	0.2861	0.1176	0.0453	0.0168
0.2	0.8086	0.5816	0.3595	0.2029	0.1078	0.0551
0.3	0.6641	0.5481	0.3945	0.2636	0.167	0.1019
0.4	0.5718	0.5203	0.4116	0.3061	0.2176	0.1494
0.5	0.5036	0.4956	0.4192	0.3355	0.2584	0.1932
0.6	0.449	0.4727	0.421	0.3555	0.2904	0.2312
0.7	0.4032	0.4506	0.419	0.3687	0.3148	0.2629
0.8	0.3637	0.4288	0.4142	0.3768	0.3331	0.2887
0.9	0.3289	0.4071	0.407	0.3811	0.3464	0.3091
1	0.2979	0.3854	0.3977	0.3821	0.3556	0.325
1.1	0.2702	0.3638	0.3867	0.3803	0.3614	0.337
1.2	0.2451	0.3424	0.3741	0.3761	0.3641	0.3455
1.3	0.2225	0.3213	0.3603	0.3697	0.3642	0.351
1.4	0.2019	0.3006	0.3453	0.3613	0.3618	0.3538
1.5	0.1833	0.2805	0.3295	0.3512	0.3572	0.354
1.6	0.1664	0.261	0.3131	0.3396	0.3505	0.3519
1.7	0.151	0.2424	0.2964	0.3267	0.342	0.3476
1.8	0.137	0.2245	0.2795	0.3129	0.3319	0.3413
1.9	0.1243	0.2076	0.2626	0.2983	0.3204	0.3332
2	0.1128	0.1915	0.246	0.2832	0.3078	0.3235
2.1	0.1023	0.1764	0.2298	0.2678	0.2944	0.3125
2.2	0.0927	0.1622	0.214	0.2523	0.2803	0.3004
2.3	0.0841	0.1489	0.1988	0.2369	0.2657	0.2874
2.4	0.0762	0.1366	0.1842	0.2217	0.251	0.2737
2.5	0.0691	0.1251	0.1704	0.2069	0.2362	0.2596
2.6	0.0626	0.1144	0.1572	0.1925	0.2216	0.2453
2.7	0.0567	0.1046	0.1449	0.1788	0.2072	0.231
2.8	0.0514	0.0955	0.1333	0.1656	0.1932	0.2167
2.9	0.0466	0.0871	0.1224	0.153	0.1797	0.2027
3	0.0422	0.0794	0.1122	0.1412	0.1667	0.1891
3.1	0.0382	0.0723	0.1028	0.13	0.1543	0.1759
3.2	0.0346	0.0659	0.0941	0.1195	0.1425	0.1632
3.3	0.0313	0.0599	0.086	0.1097	0.1314	0.1511
3.4	0.0284	0.0545	0.0785	0.1006	0.121	0.1396
3.5	0.0257	0.0495	0.0716	0.0921	0.1112	0.1288
3.6	0.0233	0.045	0.0653	0.0843	0.102	0.1186
3.7	0.0211	0.0409	0.0595	0.077	0.0935	0.109
3.8	0.0191	0.0371	0.0542	0.0703	0.0856	0.1
3.9	0.0173	0.0337	0.0493	0.0641	0.0783	0.0917
4	0.0156	0.0306	0.0448	0.0585	0.0715	0.084

Table 3. Statistical table for the probability density function of the EBSH distribution when $\theta = 0.5$.

x	$\alpha = 0.2$	$\alpha = 0.4$	$\alpha = 0.6$	$\alpha = 0.8$	$\alpha = 1$	$\alpha = 1.2$
0.1	0.5477	0.9129	1.0924	1.1444	1.1209	1.056
0.2	0.2848	0.5135	0.6707	0.7641	0.8086	0.8186
0.3	0.1933	0.3627	0.4976	0.5969	0.6641	0.7049
0.4	0.1465	0.2815	0.3987	0.4955	0.5718	0.6292
0.5	0.1179	0.2302	0.3331	0.4246	0.5036	0.5701
0.6	0.0987	0.1946	0.2858	0.3709	0.449	0.5195
0.7	0.0848	0.1684	0.2498	0.3283	0.4032	0.4742
0.8	0.0744	0.1482	0.2213	0.2932	0.3637	0.4325
0.9	0.0662	0.1322	0.1981	0.2636	0.3289	0.3937
1	0.0596	0.1192	0.1788	0.2383	0.2979	0.3575
1.1	0.0542	0.1083	0.1624	0.2164	0.2702	0.3237
1.2	0.0497	0.0992	0.1484	0.1971	0.2451	0.2922
1.3	0.0458	0.0914	0.1363	0.1801	0.2225	0.2629
1.4	0.0425	0.0846	0.1256	0.165	0.2019	0.2359
1.5	0.0397	0.0787	0.1162	0.1514	0.1833	0.211
1.6	0.0371	0.0735	0.1079	0.1392	0.1664	0.1882
1.7	0.0349	0.0688	0.1004	0.1282	0.151	0.1675
1.8	0.033	0.0647	0.0937	0.1183	0.137	0.1486
1.9	0.0312	0.061	0.0876	0.1093	0.1243	0.1316
2	0.0296	0.0576	0.0821	0.1011	0.1128	0.1162
2.1	0.0282	0.0546	0.0771	0.0936	0.1023	0.1024
2.2	0.0268	0.0518	0.0725	0.0867	0.0927	0.0901
2.3	0.0256	0.0492	0.0683	0.0804	0.0841	0.0791
2.4	0.0245	0.0469	0.0644	0.0747	0.0762	0.0693
2.5	0.0235	0.0447	0.0608	0.0694	0.0691	0.0606
2.6	0.0226	0.0427	0.0575	0.0645	0.0626	0.0529
2.7	0.0217	0.0409	0.0545	0.06	0.0567	0.0462
2.8	0.0209	0.0392	0.0516	0.0559	0.0514	0.0402
2.9	0.0202	0.0376	0.049	0.0521	0.0466	0.0349
3	0.0195	0.0361	0.0465	0.0486	0.0422	0.0303
3.1	0.0188	0.0347	0.0442	0.0453	0.0382	0.0263
3.2	0.0182	0.0334	0.0421	0.0423	0.0346	0.0228
3.3	0.0176	0.0321	0.0401	0.0395	0.0313	0.0197
3.4	0.0171	0.031	0.0382	0.0369	0.0284	0.017
3.5	0.0166	0.0299	0.0364	0.0345	0.0257	0.0147
3.6	0.0161	0.0289	0.0348	0.0323	0.0233	0.0127
3.7	0.0156	0.0279	0.0332	0.0302	0.0211	0.0109
3.8	0.0152	0.027	0.0317	0.0283	0.0191	0.0094
3.9	0.0148	0.0261	0.0304	0.0265	0.0173	0.0081
4	0.0144	0.0253	0.0291	0.0248	0.0156	0.0069

Table 4. Statistical table for the probability density function of the EBSH distribution when $\theta = 1$.

x	$\alpha = 0.2$	$\alpha = 0.4$	$\alpha = 0.6$	$\alpha = 0.8$	$\alpha = 1$	$\alpha = 1.2$
0.1	0.5878	0.8293	0.8494	0.7583	0.6245	0.4874
0.2	0.3226	0.5145	0.6	0.6132	0.5816	0.5251
0.3	0.2263	0.3861	0.4847	0.5344	0.5481	0.5365
0.4	0.1755	0.3133	0.4136	0.4807	0.5203	0.538
0.5	0.144	0.2655	0.3637	0.4397	0.4956	0.5341
0.6	0.1223	0.2312	0.3258	0.4061	0.4727	0.5265
0.7	0.1065	0.2052	0.2956	0.3774	0.4506	0.5153
0.8	0.0944	0.1847	0.2706	0.352	0.4288	0.5008
0.9	0.0848	0.168	0.2495	0.3292	0.4071	0.4831
1	0.0771	0.1542	0.2312	0.3083	0.3854	0.4625
1.1	0.0706	0.1424	0.2152	0.2891	0.3638	0.4394
1.2	0.0652	0.1323	0.2011	0.2712	0.3424	0.4144
1.3	0.0606	0.1235	0.1884	0.2545	0.3213	0.3879
1.4	0.0566	0.1158	0.1769	0.2389	0.3006	0.3607
1.5	0.0531	0.109	0.1665	0.2243	0.2805	0.3331
1.6	0.05	0.1029	0.1571	0.2106	0.261	0.3058
1.7	0.0473	0.0974	0.1484	0.1977	0.2424	0.2791
1.8	0.0448	0.0924	0.1404	0.1856	0.2245	0.2534
1.9	0.0426	0.0879	0.133	0.1743	0.2076	0.2289
2	0.0406	0.0837	0.1261	0.1636	0.1915	0.2058
2.1	0.0388	0.0799	0.1198	0.1536	0.1764	0.1842
2.2	0.0371	0.0764	0.1139	0.1442	0.1622	0.1643
2.3	0.0356	0.0732	0.1083	0.1354	0.1489	0.146
2.4	0.0342	0.0702	0.1032	0.1271	0.1366	0.1293
2.5	0.0329	0.0674	0.0983	0.1193	0.1251	0.1142
2.6	0.0317	0.0648	0.0938	0.112	0.1144	0.1005
2.7	0.0306	0.0624	0.0895	0.1052	0.1046	0.0883
2.8	0.0295	0.0601	0.0855	0.0988	0.0955	0.0773
2.9	0.0285	0.0579	0.0817	0.0927	0.0871	0.0676
3	0.0276	0.0559	0.0782	0.0871	0.0794	0.0589
3.1	0.0268	0.054	0.0748	0.0818	0.0723	0.0513
3.2	0.026	0.0523	0.0716	0.0768	0.0659	0.0446
3.3	0.0252	0.0506	0.0686	0.0722	0.0599	0.0387
3.4	0.0245	0.049	0.0657	0.0678	0.0545	0.0335
3.5	0.0238	0.0474	0.063	0.0637	0.0495	0.029
3.6	0.0232	0.046	0.0605	0.0599	0.045	0.025
3.7	0.0226	0.0446	0.058	0.0563	0.0409	0.0216
3.8	0.022	0.0433	0.0557	0.0529	0.0371	0.0186
3.9	0.0214	0.0421	0.0535	0.0497	0.0337	0.016
4	0.0209	0.0409	0.0514	0.0468	0.0306	0.0137

2.1. Model validity checking

In this regard, we shall determine if the proposed EBSH distribution is statistically valid. This can be accomplished via the strategy that follows:

$$\int_{-\infty}^{\infty} f(x)\,dx = 1. \tag{2.8}$$

To validate this, we insert Eq (2.2) into Eq (2.8).

$$\int_{-\infty}^{\infty} f(x)\,dx = \frac{\pi\alpha\theta}{2}\text{csch}\left(\frac{\pi}{2}\right)\int_{0}^{\infty} x^{\alpha-1}e^{-x^{\alpha}}\left(1-e^{-x^{\alpha}}\right)^{\theta-1}\cosh\left\{\frac{\pi}{2}\left(1-e^{-x^{\alpha}}\right)^{\theta}\right\}dx. \tag{2.9}$$

Considering Eq (2.4), Eq (2.9) can be reduced to

$$\int_{-\infty}^{\infty} f(x)\,dx = \frac{\pi\theta}{2}\text{csch}\left(\frac{\pi}{2}\right)\int_{0}^{1} w_1^{\theta-1}\cosh\left\{\frac{\pi}{2}w_1^{\theta}\right\}dw_1. \tag{2.10}$$

Based on Eq (2.6), we can express Eq (2.10) as follows:

$$\begin{aligned}\int_{-\infty}^{\infty} f(x)\,dx &= \text{csch}\left(\frac{\pi}{2}\right)\int_{0}^{\frac{\pi}{2}}\cosh(w_2)dw_2\\ &= \text{csch}\left(\frac{\pi}{2}\right)(\sinh(w_2)]_0^{\frac{\pi}{2}}\\ &= \text{csch}\left(\frac{\pi}{2}\right)\left\{\sinh\left(\frac{\pi}{2}\right)-\sinh(0)\right\}\\ &= \frac{1}{\sinh\left(\frac{\pi}{2}\right)}\left\{\sinh\left(\frac{\pi}{2}\right)\right\}\\ &= 1,\end{aligned} \tag{2.11}$$

which proves that Eq (2.8) demonstrates that the EBHS distribution is a valid probability distribution.

2.2. Survival and hazard functions

The survival function of the EBHS distribution can be derived by using Eq (2.8) as follows:

$$S(x) = 1-\text{csch}\left(\frac{\pi}{2}\right)\left\{\sinh\left(\frac{\pi}{2}\left(1-e^{-x^{\alpha}}\right)^{\theta}\right)\right\}, \qquad \theta,\alpha, \quad x>0, \tag{2.12}$$

where θ and α are the shape parameters. The hazard function of the EBSH distribution is obtained by formulating Eqs (2.2) and (2.7) as

$$h(x) = \frac{\pi\alpha\theta\text{csch}\left(\frac{\pi}{2}\right)x^{\alpha-1}e^{-x^{\alpha}}\left(1-e^{-x^{\alpha}}\right)^{\theta-1}\cosh\left\{\frac{\pi}{2}\left(1-e^{-x^{\alpha}}\right)^{\theta}\right\}}{2\left\{1-\text{csch}\left(\frac{\pi}{2}\right)\left\{\sinh\left(\frac{\pi}{2}\left(1-e^{-x^{\alpha}}\right)^{\theta}\right)\right\}\right\}}, \qquad \theta,\alpha, \quad x>0. \tag{2.13}$$

According to [36,37], the shape of the hazard function of the probability distribution is characterized by the following relation:

$$k(x) = -\frac{f'(x)}{f(x)}, \tag{2.14}$$

where $f(x)$ is the PDF of the EBSH provided in Eq (2.2), and $f'(x)$ represents partial derivatives of $f(x)$ with respect to x. Taking the partial derivatives of Eq (2.2), we get

$$f'(x) = f(x)\left\{\frac{\alpha-1}{x} - \alpha x^{\alpha-1} + \alpha(\theta-1)\left(\frac{x^{\alpha-1}e^{-x^\alpha}}{1-e^{-x^\alpha}}\right) + \frac{\pi}{2}\alpha\theta x^{\alpha-1}e^{-x^\alpha}\left(1-e^{-x^\alpha}\right)^{\theta-1}\tanh\left(\frac{\pi}{2}\left(1-e^{-x^\alpha}\right)^{\theta}\right)\right\}. \tag{2.15}$$

Inserting (2.15) into (2.14) results in the following relation:

$$k(x) = -\left(\frac{\alpha-1}{x}\right) + \alpha x^{\alpha-1} - \alpha(\theta-1)\left(\frac{x^{\alpha-1}e^{-x^\alpha}}{1-e^{-x^\alpha}}\right) - \frac{\pi}{2}\alpha\theta x^{\alpha-1}e^{-x^\alpha}\left(1-e^{-x^\alpha}\right)^{\theta-1}\tanh\left(\frac{\pi}{2}\left(1-e^{-x^\alpha}\right)^{\theta}\right). \tag{2.16}$$

To determine the hazard behavior of the EBSH distribution, the following three cases should be considered. The hazard behavior under these cases are provided in Tables 5–7.

Case I: $0 < \theta < 1$

Table 5. Asymptotic and theoretical properties for the hazard behavior of the EBSH distribution when $0 < \theta < 1$.

α	$k(x)$ as $x \to 0$	$k(x)$ as $x \to \infty$	Final output	Hazard shape
$0 < \alpha < 1$	∞	0	$k(x) \to 0$	Decreasing
$\alpha = 1$	∞	1	$k(x) \to 1$	Decreasing $\to$ constant
$\alpha > 1$	∞	∞	$k(x) \sim \alpha x^{\alpha-1} \to \infty$	Decrease $\to$ increase

Case II: $\theta = 1$

Table 6. Asymptotic and theoretical properties for the hazard behavior of the EBSH distribution when $\theta = 1$.

α	$k(x)$ as $x \to 0$	$k(x)$ as $x \to \infty$	Final output	Hazard shape
$0 < \alpha < 1$	∞	0	$k(x) \to 0$	Decreasing
$\alpha = 1$	1	1	$k(x) = 1$	Constant
$\alpha > 1$	0	∞	$k(x) \sim \alpha x^{\alpha-1} \to \infty$	Increasing

Case III: $\theta > 1$

Table 7. Asymptotic and theoretical properties for the hazard behavior of the EBSH distribution when $\theta > 1$.

α	$k(x)$ as $x \to 0$	$k(x)$ as $x \to \infty$	Final output	Hazard shape
$0 < \alpha < 1$	$-\infty$	0	$k(x) \to 0$	Increasing
$\alpha = 1$	$-\infty$	1	$k(x) \to 1$	Increasing $\to$ constant
$\alpha > 1$	$-\infty$	∞	$k(x) \sim \alpha x^{\alpha-1} \to \infty$	Increasing

2.3. Interpretation of the hazard behavior

2.3.1. Case I: $0 < \theta < 1$

For $0 < \alpha < 1$, the hazard decreases monotonically from infinity to zero, exhibiting a decreasing hazard rate or L-shaped behavior. This corresponds to the phenomenon of infant mortality, where failures are concentrated at early stages and decrease over time.

For $\alpha = 1$, the hazard decreases from infinity and converges to a constant value of one, indicating a transition from high initial risk to a stable long-term failure rate.

For $\alpha > 1$, the hazard initially decreases, attains a minimum, and then increases to infinity, producing a bathtub-shaped hazard function. This captures early failures, a period of reliability, and eventual wear-out.

2.3.2. Case II: $\theta = 1$

For $0 < \alpha < 1$, the hazard decreases from infinity to zero, corresponding to a decreasing hazard rate dominated by early failures.

For $\alpha = 1$, the hazard is constant and equal to one, representing the memoryless property of the exponential distribution.

For $\alpha > 1$, the hazard increases from zero to infinity, indicating an increasing hazard rate (IHR) associated with aging or wear-out mechanisms.

2.3.3. Case III: $\theta > 1$

For $0 < \alpha < 1$, the hazard increases toward zero; for $\alpha = 1$, it increases and approaches a constant; and for $\alpha > 1$, it increases to infinity.

Finally, the parameter α controls the global shape of the hazard function, determining whether it is decreasing, constant, increasing, or bathtub-shaped.

Figure 2 provides a graphical validation of the analytical results presented in Tables 5–7. The three subplots illustrate the flexibility of the EBSH distribution in capturing different hazard rate behaviors under varying parameter values. Figure 2(a) exhibits a monotonically increasing hazard function. This behavior is consistent with the results in Table 6 for $\theta = 1$ and $\alpha > 1$ as well as Table 7 for $\theta > 1$ and $\alpha > 1$, where the hazard function is shown to increase as $x \to \infty$. This pattern reflects wear-out failure mechanisms, where the risk of failure increases over time. The observed behavior is primarily driven by the dominance of the term $\alpha x^{\alpha-1}$ when $\alpha > 1$, which causes the hazard to grow as x increases. Figure 2(b) demonstrates a monotonically decreasing hazard function, which aligns with the results in Table 5 for $0 < \theta < 1$ and $0 < \alpha < 1$ as well as Table 6 for $\theta = 1$ and $0 < \alpha < 1$. This behavior

corresponds to the classical decreasing hazard rate or L-shaped pattern, where the failure rate is initially high and decreases over time. Such a pattern is commonly associated with infant mortality, where early failures dominate and the system stabilizes as time progresses. Figure 2(c) displays a nonmonotonic (bathtub-shaped) hazard function. This observation confirms the theoretical findings in Table 5 for $0 < \theta < 1$ and $\alpha > 1$, where the hazard initially decreases, reaches a minimum, and then increases. This type of hazard behavior is particularly important in reliability analysis, as it captures three distinct phases: early failures, a stable useful life period, and eventual wear-out failures. The graphical results in Figure 2 are in strong agreement with the analytical classifications provided in Tables 5–7. The tables describe the asymptotic and theoretical properties of the hazard function and Figure 2 provides visual confirmation of these behaviours.

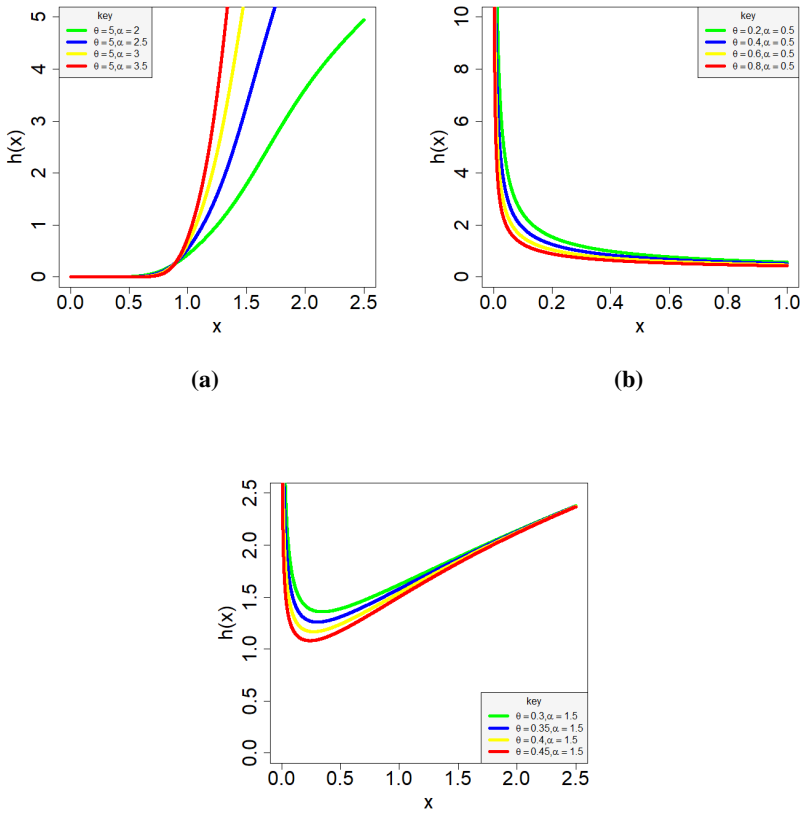

Figure 2. Hazard shapes of the EBSH distribution.

Table 8 shows that the hazard shapes of the EBSH distribution possess a decreasing failure rate when $\alpha = 0.2 - 1.2$ and $\theta = 0.5$. For the values of $\alpha = 1$ and 1.2, the shapes change direction, that is, they are characterized by decreasing-increasing-decreasing shapes.

Table 9 shows that the hazard shapes of the EBSH distribution possess a decreasing failure rate when $\alpha = 0.2 - 1.2$ and $\theta = 1$. For the values of $\alpha = 1$, the shapes change direction, that is, the shapes are characterized by a decreasing-increasing structure, whereas for $\alpha = 1$, the shapes keep going up, that is, in an increasing manner.

Table 8. Statistical table for the hazard function of the EBSH distribution when $\theta = 0.5$.

x	$\alpha = 0.2$	$\alpha = 0.4$	$\alpha = 0.6$	$\alpha = 0.8$	$\alpha = 1$	$\alpha = 1.2$
0.1	1.2507	1.6483	1.6855	1.5836	1.435	1.277
0.2	0.7134	1.0553	1.1893	1.2117	1.1766	1.1136
0.3	0.5143	0.8175	0.9826	1.0595	1.0811	1.069
0.4	0.4079	0.6836	0.863	0.9732	1.0344	1.0612
0.5	0.3409	0.5958	0.7827	0.9165	1.0089	1.0694
0.6	0.2945	0.5328	0.724	0.8757	0.9943	1.0855
0.7	0.2602	0.4851	0.6787	0.8445	0.9858	1.1054
0.8	0.2338	0.4473	0.6422	0.8196	0.981	1.1273
0.9	0.2127	0.4166	0.612	0.7992	0.9784	1.15
1	0.1955	0.3909	0.5864	0.7819	0.9774	1.1728
1.1	0.1811	0.3692	0.5644	0.767	0.9772	1.1953
1.2	0.1689	0.3504	0.5451	0.7539	0.9777	1.2172
1.3	0.1584	0.334	0.5281	0.7424	0.9785	1.2384
1.4	0.1493	0.3195	0.5128	0.7319	0.9796	1.2588
1.5	0.1413	0.3066	0.4991	0.7225	0.9808	1.2784
1.6	0.1342	0.295	0.4866	0.7139	0.982	1.2972
1.7	0.1278	0.2845	0.4752	0.7059	0.9833	1.3152
1.8	0.1221	0.275	0.4647	0.6985	0.9845	1.3323
1.9	0.117	0.2663	0.4551	0.6916	0.9857	1.3488
2	0.1123	0.2583	0.4461	0.6852	0.9869	1.3645
2.1	0.108	0.2509	0.4377	0.6791	0.9879	1.3795
2.2	0.104	0.2441	0.4299	0.6734	0.9889	1.3939
2.3	0.1004	0.2377	0.4225	0.6679	0.9899	1.4077
2.4	0.0971	0.2318	0.4156	0.6628	0.9908	1.421
2.5	0.0939	0.2262	0.4091	0.6579	0.9916	1.4338
2.6	0.0911	0.221	0.403	0.6532	0.9923	1.4461
2.7	0.0883	0.2161	0.3971	0.6487	0.993	1.4579
2.8	0.0858	0.2115	0.3916	0.6444	0.9936	1.4693
2.9	0.0835	0.2072	0.3863	0.6403	0.9942	1.4804
3	0.0812	0.2031	0.3813	0.6363	0.9947	1.491
3.1	0.0791	0.1992	0.3765	0.6325	0.9952	1.5014
3.2	0.0771	0.1955	0.3719	0.6288	0.9957	1.5114
3.3	0.0753	0.1919	0.3675	0.6252	0.9961	1.5211
3.4	0.0735	0.1886	0.3633	0.6218	0.9964	1.5306
3.5	0.0718	0.1854	0.3592	0.6184	0.9968	1.5398
3.6	0.0702	0.1823	0.3553	0.6152	0.9971	1.5488
3.7	0.0687	0.1794	0.3516	0.6121	0.9973	1.5575
3.8	0.0673	0.1766	0.348	0.609	0.9976	1.566
3.9	0.0659	0.1739	0.3445	0.6061	0.9978	1.5744
4	0.0646	0.1713	0.3411	0.6032	0.998	1.5825

Table 9. Statistical table for the hazard function of the EBSH distribution when $\theta = 1$.

x	$\alpha = 0.2$	$\alpha = 0.4$	$\alpha = 0.6$	$\alpha = 0.8$	$\alpha = 1$	$\alpha = 1.2$
0.1	0.9028	1.083	1.0049	0.8434	0.6681	0.5087
0.2	0.5304	0.7334	0.7744	0.7376	0.6651	0.5788
0.3	0.3891	0.5875	0.6721	0.6902	0.67	0.6282
0.4	0.3126	0.5033	0.6114	0.6642	0.6803	0.6723
0.5	0.2638	0.4472	0.5703	0.6487	0.6941	0.7154
0.6	0.2297	0.4064	0.54	0.639	0.7102	0.7591
0.7	0.2044	0.375	0.5165	0.6328	0.7274	0.8034
0.8	0.1847	0.35	0.4975	0.6287	0.7451	0.848
0.9	0.169	0.3294	0.4816	0.6259	0.7628	0.8923
1	0.156	0.312	0.468	0.6241	0.7801	0.9361
1.1	0.1452	0.2972	0.4563	0.6227	0.7968	0.9787
1.2	0.1359	0.2842	0.4459	0.6217	0.8127	1.02
1.3	0.1279	0.2729	0.4366	0.6208	0.8278	1.0596
1.4	0.121	0.2628	0.4281	0.6201	0.842	1.0973
1.5	0.1148	0.2537	0.4205	0.6194	0.8552	1.1331
1.6	0.1094	0.2455	0.4134	0.6187	0.8676	1.1669
1.7	0.1045	0.2381	0.4069	0.6179	0.879	1.1988
1.8	0.1001	0.2313	0.4008	0.6171	0.8896	1.2287
1.9	0.0961	0.225	0.3951	0.6162	0.8993	1.2567
2	0.0924	0.2192	0.3898	0.6153	0.9083	1.283
2.1	0.0891	0.2138	0.3848	0.6142	0.9165	1.3075
2.2	0.086	0.2088	0.38	0.6131	0.924	1.3305
2.3	0.0832	0.2042	0.3755	0.612	0.9309	1.3519
2.4	0.0806	0.1998	0.3712	0.6107	0.9372	1.3721
2.5	0.0781	0.1957	0.367	0.6094	0.943	1.3909
2.6	0.0758	0.1918	0.3631	0.6081	0.9482	1.4086
2.7	0.0737	0.1882	0.3593	0.6067	0.953	1.4252
2.8	0.0717	0.1847	0.3557	0.6052	0.9573	1.4408
2.9	0.0698	0.1814	0.3522	0.6037	0.9613	1.4556
3	0.0681	0.1783	0.3489	0.6022	0.9649	1.4695
3.1	0.0664	0.1753	0.3456	0.6006	0.9682	1.4827
3.2	0.0648	0.1725	0.3425	0.599	0.9711	1.4952
3.3	0.0634	0.1698	0.3395	0.5974	0.9738	1.5071
3.4	0.0619	0.1672	0.3366	0.5958	0.9763	1.5185
3.5	0.0606	0.1648	0.3337	0.5941	0.9785	1.5294
3.6	0.0593	0.1624	0.331	0.5924	0.9805	1.5398
3.7	0.0581	0.1601	0.3283	0.5907	0.9824	1.5498
3.8	0.057	0.1579	0.3257	0.5891	0.984	1.5594
3.9	0.0559	0.1558	0.3232	0.5874	0.9855	1.5686
4	0.0548	0.1538	0.3207	0.5856	0.9869	1.5776

3. Properties of the EBSH distribution

This section discusses the structural features of the EBSH distribution, such as linear representations, quantile function, moments, and probability weighted moments.

3.1. Linear representations

The PDF of the proposed EBSH distribution can be given in linear form using the following procedure:

Consider the power series expansion of hyperbolic functions

$$\cosh(z) = \sum_{j=0}^{\infty} \frac{z^{2j}}{(2j)!} \tag{3.1}$$

and

$$\sinh(z) = \sum_{i=0}^{\infty} \frac{z^{2i+1}}{(2i+1)!}. \tag{3.2}$$

Applying Eq (3.1) to the PDF provided in Eq (2.2),

$$\begin{aligned} f(x) &= \frac{\pi\alpha\theta}{2}\operatorname{csch}\left(\frac{\pi}{2}\right)x^{\alpha-1}e^{-x^{\alpha}}\left(1-e^{-x^{\alpha}}\right)^{\theta-1}\sum_{j=0}^{\infty}\frac{\left\{\frac{\pi}{2}\left(1-e^{-x^{\alpha}}\right)^{\theta}\right\}^{2j}}{(2j)!} \\ &= \frac{\pi\alpha\theta}{2}\operatorname{csch}\left(\frac{\pi}{2}\right)x^{\alpha-1}e^{-x^{\alpha}}\sum_{j=0}^{\infty}\frac{\left(\frac{\pi}{2}\right)^{2j}}{(2j)!}\left(1-e^{-x^{\alpha}}\right)^{\theta(2j+1)-1}. \end{aligned} \tag{3.3}$$

Consider the binomial expansion for $\vartheta > 0$ and $|z| < 1$; then, the series expansion holds:

$$(1-z)^{\vartheta} = \sum_{l=0}^{\infty}\frac{(-1)^l}{l!}\binom{\vartheta}{l}z^l. \tag{3.4}$$

Using Eq (3.4), the PDF of Eq (3.3) becomes

$$\begin{aligned} f(x) &= \frac{\pi\alpha\theta}{2}\operatorname{csch}\left(\frac{\pi}{2}\right)x^{\alpha-1}e^{-x^{\alpha}}\sum_{j=0}^{\infty}\frac{\left(\frac{\pi}{2}\right)^{2j}}{(2j)!}\sum_{l=0}^{\infty}\frac{(-1)^l}{l!}\binom{\theta(2j+1)-1}{l}\left(e^{-x^{\alpha}}\right)^l \\ &= \frac{\pi\alpha\theta}{2}\operatorname{csch}\left(\frac{\pi}{2}\right)x^{\alpha-1}\sum_{j,l=0}^{\infty}\frac{\left(\frac{\pi}{2}\right)^{2j}\frac{(-1)^l}{l!}}{(2j)!}\binom{\theta(2j+1)-1}{l}e^{-(1+l)x^{\alpha}}. \end{aligned} \tag{3.5}$$

The infinite series representations derived in this section converge rapidly due to the exponential decay induced by the term $e^{-(1+l)x^{\alpha}}$. In practical computations, only a finite number of terms are required to achieve high numerical accuracy, which makes the representation computationally efficient for applied use. The tail behavior of the EBSH distribution is primarily governed by the exponential term $e^{-x^{\alpha}}$. As $x \to \infty$, this term dominates, causing the PDF to decay exponentially. This indicates that the EBSH distribution belongs to the class of light-tailed distributions. However, the parameters α and θ provide sufficient flexibility to control the rate of decay, which allows the model to approximate moderately heavy-tailed behavior in practical applications. This property enhances its suitability for modeling real-world data where extreme values may occur but are not dominant.

3.2. Quantile function

To determine the quantile function of the EBSH distribution, invert the CDF in Eq (2.7) as follows: Let

$$u = \operatorname{csch}\left(\frac{\pi}{2}\right)\left\{\sinh\left(\frac{\pi}{2}\left(1-e^{-x_{q(u)}^{\alpha}}\right)^{\theta}\right)\right\} = \frac{1}{\sinh\left(\frac{\pi}{2}\right)}\left\{\sinh\left(\frac{\pi}{2}\left(1-e^{-x_{q(u)}^{\alpha}}\right)^{\theta}\right)\right\}, \quad 0 < u < 1. \tag{3.6}$$

This indicates that

$$\left\{\sinh\left(\frac{\pi}{2}\left(1-e^{-x_{q(u)}^{\alpha}}\right)^{\theta}\right)\right\} = u\sinh\left(\frac{\pi}{2}\right). \tag{3.7}$$

Taking the inverse hyperbolic sine on both sides of Eq (3.7) yields

$$\frac{\pi}{2}\left(1-e^{-x_{q(u)}^{\alpha}}\right)^{\theta} = \sinh^{-1}\left\{u\sinh\left(\frac{\pi}{2}\right)\right\}. \tag{3.8}$$

Further simplifying Eq (3.8) provides

$$e^{-x_{q(u)}^{\alpha}} = 1-\left\{\frac{2}{\pi}\sinh^{-1}\left\{u\sinh\left(\frac{\pi}{2}\right)\right\}\right\}^{\frac{1}{\theta}}. \tag{3.9}$$

Taking the logarithm of both sides of Eq (3.9) leads to

$$x_{q(u)}^{\alpha} = -\log\left\{1-\left\{\frac{2}{\pi}\sinh^{-1}\left\{u\sinh\left(\frac{\pi}{2}\right)\right\}\right\}^{\frac{1}{\theta}}\right\}. \tag{3.10}$$

The quantile function is obtained as follows:

$$x_{q(u)} = \left\{-\log\left\{1-\left\{\frac{2}{\pi}\sinh^{-1}\left\{u\sinh\left(\frac{\pi}{2}\right)\right\}\right\}^{\frac{1}{\theta}}\right\}\right\}^{\frac{1}{\alpha}}. \tag{3.11}$$

Using Eq (3.11), the first, second, and third quartiles of the EBSH distribution can be expressed as follows:

$$x_{q(\frac{1}{4})} = \left\{-\log\left\{1-\left\{\frac{2}{\pi}\sinh^{-1}\left\{\frac{1}{4}\sinh\left(\frac{\pi}{2}\right)\right\}\right\}^{\frac{1}{\theta}}\right\}\right\}^{\frac{1}{\alpha}}, \tag{3.12}$$

$$x_{q(\frac{1}{2})} = \left\{-\log\left\{1-\left\{\frac{2}{\pi}\sinh^{-1}\left\{\frac{1}{2}\sinh\left(\frac{\pi}{2}\right)\right\}\right\}^{\frac{1}{\theta}}\right\}\right\}^{\frac{1}{\alpha}}, \tag{3.13}$$

and

$$x_{q(\frac{3}{4})} = \left\{-\log\left\{1-\left\{\frac{2}{\pi}\sinh^{-1}\left\{\frac{3}{4}\sinh\left(\frac{\pi}{2}\right)\right\}\right\}^{\frac{1}{\theta}}\right\}\right\}^{\frac{1}{\alpha}}. \tag{3.14}$$

3.3. Moments

Statistical moments play a central role in characterizing a probability distribution, capturing its location, dispersion, skewness, and kurtosis. In addition to summarizing the shape and variability of a distribution, moments also form the basis for the derivation of further properties, providing both concise descriptive measures and deeper analytical insight into distributional behavior.

The moments of the EBSH distribution are derived based on the PDF given in Eq (3.5).

$$E\left(X^r\right) = \frac{\pi\alpha\theta}{2}\operatorname{csch}\left(\frac{\pi}{2}\right)\sum_{j,l=0}^{\infty}\frac{\left(\frac{\pi}{2}\right)^{2j}\frac{(-1)^l}{l!}}{(2j)!}\binom{\theta(2j+1)-1}{l}\int_0^{\infty}x^{r+\alpha-1}e^{-(1+l)x^{\alpha}}dx. \tag{3.15}$$

Let

$$w_3 = (1+l)\,x^{\alpha}, \quad \text{which implies} \quad dx = \frac{1}{\alpha\,(1+l)\,x^{\alpha-1}}dw_3. \tag{3.16}$$

Following Eq (3.16), Eq (3.15) yields

$$\begin{aligned}
E\left(X^r\right) &= \frac{\pi\theta}{2}\operatorname{csch}\left(\frac{\pi}{2}\right)\sum_{j,l=0}^{\infty}\frac{\left(\frac{\pi}{2}\right)^{2j}\frac{(-1)^l}{l!}}{(2j)!\,(1+l)}\binom{\theta(2j+1)-1}{l}\int_0^{\infty}\left\{\left(\frac{w_3}{l+1}\right)^{\frac{1}{\alpha}}\right\}^r e^{-w_3}dw_3\\
&= \frac{\pi\theta}{2}\operatorname{csch}\left(\frac{\pi}{2}\right)\sum_{j,l=0}^{\infty}\frac{\left(\frac{\pi}{2}\right)^{2j}\frac{(-1)^l}{l!}}{(2j)!\,(1+l)^{1+\frac{r}{\alpha}}}\binom{\theta(2j+1)-1}{l}\int_0^{\infty}w_3^{\frac{r}{\alpha}}e^{-w_3}dw_3\\
&= \frac{\pi\theta}{2}\operatorname{csch}\left(\frac{\pi}{2}\right)\sum_{j,l=0}^{\infty}\frac{\left(\frac{\pi}{2}\right)^{2j}\frac{(-1)^l}{l!}}{(2j)!\,(1+l)^{1+\frac{r}{\alpha}}}\binom{\theta(2j+1)-1}{l}\int_0^{\infty}w_3^{\left(1+\frac{r}{\alpha}\right)-1}e^{-w_3}dw_3\\
&= \frac{\pi\theta}{2}\operatorname{csch}\left(\frac{\pi}{2}\right)\sum_{j,l=0}^{\infty}\frac{\left(\frac{\pi}{2}\right)^{2j}\frac{(-1)^l}{l!}}{(2j)!\,(1+l)^{1+\frac{r}{\alpha}}}\binom{\theta(2j+1)-1}{l}\Gamma\left(1+\frac{r}{\alpha}\right).
\end{aligned} \tag{3.17}$$

The first four moments of the EBSH distribution are determined by setting $r = 1, 2, 3$, and 4 given as

$$E\left(X\right) = \frac{\pi\theta}{2}\operatorname{csch}\left(\frac{\pi}{2}\right)\sum_{j,l=0}^{\infty}\frac{\left(\frac{\pi}{2}\right)^{2j}\frac{(-1)^l}{l!}}{(2j)!\,(1+l)^{1+\frac{1}{\alpha}}}\binom{\theta(2j+1)-1}{l}\Gamma\left(1+\frac{1}{\alpha}\right), \tag{3.18}$$

$$E\left(X^2\right) = \frac{\pi\theta}{2}\operatorname{csch}\left(\frac{\pi}{2}\right)\sum_{j,l=0}^{\infty}\frac{\left(\frac{\pi}{2}\right)^{2j}\frac{(-1)^l}{l!}}{(2j)!\,(1+l)^{1+\frac{2}{\alpha}}}\binom{\theta(2j+1)-1}{l}\Gamma\left(1+\frac{2}{\alpha}\right), \tag{3.19}$$

$$E\left(X^3\right) = \frac{\pi\theta}{2}\operatorname{csch}\left(\frac{\pi}{2}\right)\sum_{j,l=0}^{\infty}\frac{\left(\frac{\pi}{2}\right)^{2j}\frac{(-1)^l}{l!}}{(2j)!\,(1+l)^{1+\frac{3}{\alpha}}}\binom{\theta(2j+1)-1}{l}\Gamma\left(1+\frac{3}{\alpha}\right), \tag{3.20}$$

and

$$E\left(X^4\right) = \frac{\pi\theta}{2}\operatorname{csch}\left(\frac{\pi}{2}\right)\sum_{j,l=0}^{\infty}\frac{\left(\frac{\pi}{2}\right)^{2j}\frac{(-1)^l}{l!}}{(2j)!\,(1+l)^{1+\frac{4}{\alpha}}}\binom{\theta(2j+1)-1}{l}\Gamma\left(1+\frac{4}{\alpha}\right). \tag{3.21}$$

Equation (3.18) produces the mean of the EBSH distribution, whereas Eqs (3.18) and (3.19) express the variance as

$$v(X) = \sum_{j,l=0}^{\infty} \varpi_{j,l} \frac{\Gamma\left(1+\frac{2}{\alpha}\right)}{(1+l)^{1+\frac{2}{\alpha}}} - \left\{ \sum_{j,l=0}^{\infty} \varpi_{j,l} \frac{\Gamma\left(1+\frac{1}{\alpha}\right)}{(1+l)^{1+\frac{1}{\alpha}}} \right\}^2, \tag{3.22}$$

where

$$\varpi_{j,l} = \frac{\pi\theta}{2} \operatorname{csch}\left(\frac{\pi}{2}\right) \frac{\left(\frac{\pi}{2}\right)^{2j} \frac{(-1)^l}{l!}}{(2j)!} \binom{\theta(2j+1)-1}{l}.$$

The skewness and kurtosis are computed using the moments of the EBSH distribution as follows.

3.3.1. Skewness

The skewness of the EBSH distribution is derived as

$$\text{skewness} = \frac{E\left(X^3\right) - 3\mu E\left(X^2\right) + 2\mu^3}{\{v(X)\}^{\frac{3}{2}}}, \tag{3.23}$$

where μ is the mean of the EBSH distribution provided in Eq (3.18).

3.3.2. Kurtosis

The kurtosis of the EBSH distribution is obtained as

$$\text{kurtosis} = \frac{E\left(X^4\right) - 4\mu E\left(X^3\right) + 6\mu^2 E\left(X^2\right) - 4E\left(X^4\right) + \mu^4}{\{v(X)\}^2}. \tag{3.24}$$

From Table 10, irrespective of the value of the parameters, the skewnesses are all negative and below -1, which signifies that the distribution has a left-skewed shape. Furthermore, this highlights that the EBSH distribution can equally model left-asymmetric datasets. The values for the kurtosis show that the EBSH distribution is leptokurtic, which means in comparison to a normal distribution, it features a sharper peak and heavier tails.

From Table 11, irrespective of the value of the parameters, the skewnesses are all positive and above one, which signifies that the distribution has a right-skewed shape. Furthermore, this highlights that the EBSH distribution can equally model right-asymmetric datasets. The values for the kurtosis show that the EBSH distribution is leptokurtic, which means in comparison to a normal distribution, it features a sharper peak and heavier tails.

Table 10. Skewness and kurtosis of the EBSH distribution when $\alpha > 1$.

α	θ	Skewness	Kurtosis	α	θ	Skewness	Kurtosis
5	1	-0.4473	3.0500	10	1	-0.8254	3.9343
5	2	-0.3396	3.0862	10	2	-0.5929	3.5400
5	3	-0.2499	3.0435	10	3	-0.4533	3.3180
5	4	-0.1850	3.0135	10	4	-0.3619	3.1970
6	1	-0.5641	3.2648	11	1	-0.8647	4.0587
6	2	-0.4209	3.2049	11	2	-0.6174	3.5975
6	3	-0.3161	3.1158	11	3	-0.4725	3.3521
6	4	-0.2430	3.0610	11	4	-0.3783	3.2201
7	1	-0.6527	3.4617	12	1	-0.8981	4.1699
7	2	-0.4808	3.3084	12	2	-0.6382	3.6479
7	3	-0.3643	3.1788	12	3	-0.4887	3.3820
7	4	-0.2850	3.1031	12	4	-0.3923	3.2406
8	1	-0.7224	3.6381	13	1	-0.9271	4.2699
8	2	-0.5267	3.3974	13	2	-0.6559	3.6924
8	3	-0.4010	3.2325	13	3	-0.5029	3.4084
8	4	-0.3168	3.1393	13	4	-0.4057	3.2597
9	1	-0.7788	3.7949	14	1	-0.9523	4.3601
9	2	-0.5632	3.4739	14	2	-0.6710	3.7316
9	3	-0.4299	3.2785	14	3	-0.5148	3.4307
9	4	-0.3418	3.1704	14	4	-0.4189	3.2757

Table 11. Skewness and kurtosis of the EBSH distribution when $\alpha \leq 1$.

α	θ	Skewness	Kurtosis	α	θ	Skewness	Kurtosis
0.1	1	4.501283	23.93139	0.6	1	2.400335	10.30185
0.1	2	4.332662	21.81136	0.6	2	1.890723	7.021077
0.1	3	4.591294	23.9231	0.6	3	1.59275	5.594593
0.1	4	4.941862	27.29965	0.6	4	1.417685	4.854616
0.2	1	2.819375	10.74377	0.7	1	2.463202	11.81342
0.2	2	2.716158	9.376308	0.7	2	1.993106	8.520282
0.2	3	2.918136	10.00271	0.7	3	1.738785	7.1098
0.2	4	3.089598	10.76596	0.7	4	1.589017	6.350584
0.3	1	2.171164	7.357281	0.8	1	2.231446	10.82024
0.3	2	2.048711	6.0873	0.8	2	1.835718	8.330503
0.3	3	2.150347	6.055155	0.8	3	1.647417	7.344843
0.3	4	2.245104	6.162339	0.8	4	1.541919	6.826327
0.4	1	2.016216	6.894106	0.9	1	1.903521	8.650035
0.4	2	1.736889	5.138388	0.9	2	1.559001	6.940302
0.4	3	1.644077	4.537298	0.9	3	1.413943	6.338744
0.4	4	1.64221	4.319532	0.9	4	1.335982	6.039047
0.5	1	2.160063	8.090417	1	1	1.625469	6.954915
0.5	2	1.716814	5.541032	1	2	1.318385	5.751383
0.5	3	1.462901	4.462884	1	3	1.20089	5.371465
0.5	4	1.334989	3.953698	1	4	1.139547	5.190684

3.4. Probability weighted moments

The probability weighted moments (PWM) of the EBSH distribution are presented as

$$\mathrm{P}_{r,1} = \mathrm{E}\left(X^r \{F(X)\}\right) = \int_{-\infty}^{\infty} x^r f(x) F(x)\, dx, \tag{3.25}$$

where $f(x)$ and $F(x)$ are the PDF and CDF of the EBSH distribution defined in Eqs (2.2) and (2.7). Now, let us simplify the PDF and CDF in Eq (3.25).

$$f(x) F(x) = f(x) \operatorname{csch}\left(\frac{\pi}{2}\right)\left\{\sinh\left(\frac{\pi}{2}\left(1 - e^{-x^\alpha}\right)^\theta\right)\right\}. \tag{3.26}$$

Applying Eq (3.2) to Eq (3.26),

$$f(x) F(x) = f(x) \operatorname{csch}\left(\frac{\pi}{2}\right) \sum_{i=0}^{\infty} \frac{\left\{\frac{\pi}{2}\left(1 - e^{-x^\alpha}\right)^\theta\right\}^{2i+1}}{(2i+1)!}. \tag{3.27}$$

Consider the PDF in Eq (3.3). Then, Eq (3.27) becomes

$$f(x) F(x) = \frac{\pi\alpha\theta}{2}\left\{\operatorname{csch}\left(\frac{\pi}{2}\right)\right\}^2 x^{\alpha-1} e^{-x^\alpha} \sum_{j,i=0}^{\infty} \frac{\left(\frac{\pi}{2}\right)^{2j+2i+1}}{(2j)!\,(2i+1)!}\left(1 - e^{-x^\alpha}\right)^{\theta(2j+1)+2i}. \tag{3.28}$$

Applying Eqs (3.4) and (3.28) yields

$$\begin{aligned} f(x) F(x) &= \frac{\pi\alpha\theta}{2}\left\{\operatorname{csch}\left(\frac{\pi}{2}\right)\right\}^2 x^{\alpha-1} e^{-x^\alpha} \sum_{j,i=0}^{\infty} \frac{\left(\frac{\pi}{2}\right)^{2j+2i+1}}{(2j)!\,(2i+1)!} \sum_{l=0}^{\infty} \frac{(-1)^l}{l!}\binom{\theta(2j+1)+2i}{l}\left\{e^{-x^\alpha}\right\}^l \\ &= \frac{\pi\alpha\theta}{2}\left\{\operatorname{csch}\left(\frac{\pi}{2}\right)\right\}^2 x^{\alpha-1} \sum_{j,i,l=0}^{\infty} \frac{\left(\frac{\pi}{2}\right)^{2j+2i+1}(-1)^l}{(2j)!\,(2i+1)!\,l!}\binom{\theta(2j+1)+2i}{l} e^{-(1+l)x^\alpha} \\ &= x^{\alpha-1} \sum_{j,i,l=0}^{\infty} \varphi_{j,i,l}\, e^{-(1+l)x^\alpha}, \end{aligned} \tag{3.29}$$

where

$$\varphi_{j,i,l} = \frac{\pi\alpha\theta}{2}\left\{\operatorname{csch}\left(\frac{\pi}{2}\right)\right\}^2 \frac{\left(\frac{\pi}{2}\right)^{2j+2i+1}(-1)^l}{(2j)!\,(2i+1)!\,l!}\binom{\theta(2j+1)+2i}{l}.$$

Thus, the PWM of the EBSH distribution is derived by substituting Eq (3.29) into Eq (3.25).

$$\mathrm{P}_{r,1} = \sum_{j,i,l=0}^{\infty} \varphi_{j,i,l} \int_0^{\infty} x^{r+\alpha-1} e^{-(1+l)x^\alpha} dx. \tag{3.30}$$

Using Eq (3.16), Eq (3.30) leads to

$$\mathrm{P}_{r,1} = \frac{1}{\alpha} \sum_{j,i,l=0}^{\infty} \frac{\varphi_{j,i,l}}{(1+l)^{1+\frac{r}{\alpha}}} \int_0^{\infty} w_3^{\frac{r}{\alpha}} e^{-w_3} dw_3$$

$$= \frac{1}{\alpha}\sum_{j,i,l=0}^{\infty}\frac{\varphi_{j,i,l}}{(1+l)^{1+\frac{r}{\alpha}}}\int_0^{\infty} w_3^{\left(1+\frac{r}{\alpha}\right)-1}e^{-w_3}dw_3$$

$$= \frac{1}{\alpha}\sum_{j,i,l=0}^{\infty}\frac{\varphi_{j,i,l}}{(1+l)^{1+\frac{r}{\alpha}}}\Gamma\left(1+\frac{r}{\alpha}\right). \tag{3.31}$$

4. Parameter estimation

This section presents the maximum likelihood estimator (MLE) procedure for estimating the unknown parameters of the proposed EBSH distribution. Let the random variables $X_1, X_2, \ldots, X_n$ be drawn from the random sample of the EBSH model with PDF $f(x)$ as defined in Eq (2.2). To determine the model parameters, the likelihood function of Eq (2.2) denoted by (L) is given as

$$\ell = \left\{\frac{\pi\alpha\theta}{2}\text{csch}\left(\frac{\pi}{2}\right)\right\}^n\prod_{i=1}^{n}\left\{x_i^{\alpha-1}e^{-x_i^{\alpha}}\left(1-e^{-x_i^{\alpha}}\right)^{\theta-1}\cosh\left\{\frac{\pi}{2}\left(1-e^{-x_i^{\alpha}}\right)^{\theta}\right\}\right\}. \tag{4.1}$$

The log-likelihood function of Eq (4.1) is obtained as follows:

$$\begin{aligned}\ell\ell =& n\log(\pi)+n\log(\alpha)+n\log(\theta)-n\log(2)+n\log\left(\text{csch}\left(\frac{\pi}{2}\right)\right)+(\alpha-1)\sum_{i=1}^{n}\log(x_i)-\sum_{i=1}^{n}(x_i^{\alpha})\\ &+(\theta-1)\sum_{i=1}^{n}\log\left(1-e^{-x_i^{\alpha}}\right)+\sum_{i=1}^{n}\log\left\{\cosh\left\{\frac{\pi}{2}\left(1-e^{-x_i^{\alpha}}\right)^{\theta}\right\}\right\}.\end{aligned} \tag{4.2}$$

Henceforth, the estimates of the model parameters will be obtained by differentiating Eq (4.2) about the parameters α and θ as follows:

$$\begin{aligned}\frac{\partial\ell}{\partial\alpha} =& \frac{n}{\alpha}+\sum_{i=1}^{n}\log(x_i)-\sum_{i=1}^{n}(x_i^{\alpha})\log(x_i)+(\theta-1)\sum_{i=1}^{n}\left(\frac{\frac{\partial}{\partial\alpha}\left(1-e^{-x_i^{\alpha}}\right)}{1-e^{-x_i^{\alpha}}}\right)+\sum_{i=1}^{n}\left(\frac{\frac{\partial}{\partial\alpha}\left(\cosh\left\{\frac{\pi}{2}\left(1-e^{-x_i^{\alpha}}\right)^{\theta}\right\}\right)}{\cosh\left\{\frac{\pi}{2}\left(1-e^{-x_i^{\alpha}}\right)^{\theta}\right\}}\right)\\ =& \frac{n}{\alpha}+\sum_{i=1}^{n}\log(x_i)-\sum_{i=1}^{n}(x_i^{\alpha})\log(x_i)+(\theta-1)\sum_{i=1}^{n}\left(\frac{x_i^{\alpha}\log(x_i)\,e^{-x_i^{\alpha}}}{1-e^{-x_i^{\alpha}}}\right)\\ &+\frac{\pi}{2}\sum_{i=1}^{n}\left(\frac{x_i^{\alpha}\log(x_i)\,e^{-x_i^{\alpha}}\left(1-e^{-x_i^{\alpha}}\right)^{\theta-1}\sinh\left\{\frac{\pi}{2}\left(1-e^{-x_i^{\alpha}}\right)^{\theta}\right\}}{\cosh\left\{\frac{\pi}{2}\left(1-e^{-x_i^{\alpha}}\right)^{\theta}\right\}}\right)\end{aligned} \tag{4.3}$$

and

$$\begin{aligned}\frac{\partial\ell}{\partial\theta} =& \frac{n}{\theta}+\sum_{i=1}^{n}\log\left(1-e^{-x_i^{\alpha}}\right)+\sum_{i=1}^{n}\left(\frac{\frac{\partial}{\partial\theta}\left(\cosh\left\{\frac{\pi}{2}\left(1-e^{-x_i^{\alpha}}\right)^{\theta}\right\}\right)}{\cosh\left\{\frac{\pi}{2}\left(1-e^{-x_i^{\alpha}}\right)^{\theta}\right\}}\right)\\ =& \frac{n}{\theta}+\sum_{i=1}^{n}\log\left(1-e^{-x_i^{\alpha}}\right)+\frac{\pi}{2}\sum_{i=1}^{n}\left(\frac{\sinh\left\{\frac{\pi}{2}\left(1-e^{-x_i^{\alpha}}\right)^{\theta}\right\}\left(1-e^{-x_i^{\alpha}}\right)^{\theta}\log\left(1-e^{-x_i^{\alpha}}\right)}{\cosh\left\{\frac{\pi}{2}\left(1-e^{-x_i^{\alpha}}\right)^{\theta}\right\}}\right).\end{aligned} \tag{4.4}$$

Setting Eqs (4.3) and (4.4) to zero and then simplifying results in parameter estimates for the EBSH distribution. This will be accomplished through the execution of the Newton-Raphson algorithm with suitable packages such as R and MATLAB.

To ensure numerical stability during maximum likelihood estimation, it is important to note that the arguments of the hyperbolic functions in the EBSH distribution are naturally bounded. Specifically,

$$z = \frac{\pi}{2}\left(1 - e^{-x^{\alpha}}\right)^{\theta}, \quad 0 < z < \frac{\pi}{2}, \tag{4.5}$$

implying that the values of $\cosh(z)$ and $\sinh(z)$ remain finite for all admissible parameter values. This prevents numerical overflow even when θ and α are relatively large. Furthermore, the log-likelihood function is evaluated using stable log-scale computations such as $\log(\cosh(z))$ together with parameter constraints and convergence controls within the Newton-Raphson algorithm to ensure reliable optimization.

5. Simulation

Here, the effectiveness of the estimation processes in estimating the EBSH parameters is assessed by Monte Carlo simulation studies. The steps of the simulation algorithm are explained as follows:

i. Set the initial values of the parameters θ and α, and define the sample size n;
ii. Produce a random sample of size n from the EBSH distribution using Eq (3.11);
iii. Compute the model parameter estimates; and
iv. Repeat the process 2 and 3 N times. N = 1000 Monte Carlo replications were used in the simulation, which was run using the R software.

We take into account various values for the model parameters and sample sizes $n = 5, 10, 20, 30, 50, 100, 200, 500$, and 1000. For each, the maximum likelihood (ML), least-square (LS), and weighted least-square (WLS) estimates were evaluated using the mean and mean square error (MSE), which are calculated from 1000 Monte Carlo replications. The numerical findings for the mean and MSE of the estimates derived from the various estimation techniques are presented in Tables 12–14. Interesting information is revealed by these results. It should be noted that the estimates of the EBSH parameters derived from the estimation techniques perform rather well, showing minimal bias and reasonable MSEs in every scenario taken into consideration; in other words, these estimates are fairly stable and, more significantly, relatively near to the actual values. Furthermore, when the sample size increases, the MSE decreases, suggesting that these estimators are reliable. To put it briefly, all estimation techniques yield consistent and asymptotically unbiased estimators for the EBSH parameters. Hence, the MLE approach has the lowest MSE as sample size increases; it offers more consistent and dependable parameter estimates in this study.

Table 12. Simulation results for the EBSH distribution when $\theta = 1$ and $\alpha = 1$.

		LSE		WSLE		MLE	
n	Parameter	Mean	MSE	Mean	MSE	Mean	MSE
5	θ	1.4864	3.2870	1.2389	1.2932	1.3437	1.6362
	α	1.7322	2.8934	1.0865	0.6365	1.6746	3.1544
10	θ	1.1129	0.4085	1.0818	0.3362	1.1173	0.3599
	α	1.1643	0.4786	1.0315	0.2650	1.2180	0.5344
20	θ	1.0406	0.1223	1.0329	0.1117	1.0507	0.1067
	α	1.0366	0.0714	1.0157	0.0580	1.0837	0.0506
30	θ	1.0154	0.0686	1.0133	0.0640	1.0265	0.0626
	α	1.0156	0.0370	1.0113	0.0303	1.0553	0.0273
50	θ	1.0056	0.0395	1.0056	0.0374	1.0153	0.0355
	α	1.0050	0.0194	1.0082	0.0161	1.0310	0.0132
100	θ	1.0051	0.0192	1.0047	0.0175	1.0078	0.0155
	α	1.0010	0.0084	1.0054	0.0069	1.0164	0.0059
200	θ	1.0020	0.0086	1.0018	0.0078	1.0030	0.0070
	α	0.9996	0.0042	1.0030	0.0033	1.0076	0.0028
500	θ	1.0019	0.0036	1.0016	0.0032	1.0019	0.0028
	α	1.0000	0.0016	1.0013	0.0013	1.0030	0.0010
1000	θ	1.0023	0.0018	1.0020	0.0016	1.0015	0.0014
	α	1.0006	0.0008	1.0010	0.0006	1.0016	0.0005

Table 13. Simulation results for the EBSH distribution when $\theta = 1.5$ and $\alpha = 1$.

		LSE		WSLE		MLE	
n	Parameter	Mean	MSE	Mean	MSE	Mean	MSE
5	θ	2.5809	10.5406	1.8831	3.4256	1.7478	0.9757
	α	1.5823	2.2692	1.0448	0.4580	1.1359	0.1429
10	θ	1.7263	1.1247	1.6157	0.8045	2.2867	7.2566
	α	1.1000	0.1606	1.0024	0.1033	1.4189	1.4275
20	θ	1.5688	0.2835	1.5496	0.2593	1.6074	0.2473
	α	1.0226	0.0449	1.0072	0.0398	1.0633	0.0311
30	θ	1.5248	0.1510	1.5202	0.1410	1.5607	0.1407
	α	1.0078	0.0238	1.0056	0.0205	1.0429	0.0180
50	θ	1.5078	0.0848	1.5094	0.0805	1.5346	0.0774
	α	1.0014	0.0130	1.0046	0.0110	1.0246	0.0093
100	θ	1.5064	0.0402	1.5079	0.0367	1.5179	0.0332
	α	0.9995	0.0058	1.0035	0.0048	1.0130	0.0042
200	θ	1.5022	0.0185	1.5036	0.0168	1.5075	0.0153
	α	0.9990	0.0029	1.0020	0.0024	1.0060	0.0020
500	θ	1.5026	0.0076	1.5027	0.0069	1.5040	0.0060
	α	0.9998	0.0011	1.0009	0.0009	1.0023	0.0008
1000	θ	1.5037	0.0038	1.5034	0.0034	1.5028	0.0030
	α	1.0004	0.0006	1.0007	0.0005	1.0012	0.0004

Table 14. Simulation results for the EBSH distribution when $\theta = 1$ and $\alpha = 2$.

		LSE		WSLE		MLE	
n	Parameter	Mean	MSE	Mean	MSE	Mean	MSE
5	θ	1.5128	3.8955	1.2493	1.4721	1.3439	1.6363
	α	3.4549	12.5789	2.1415	2.2813	3.4053	15.4650
10	θ	1.1126	0.4048	1.0804	0.3251	1.1176	0.3594
	α	2.3169	1.5206	2.0625	1.0132	2.4228	1.7635
20	θ	1.0399	0.1224	1.0326	0.1125	1.0515	0.1081
	α	2.0827	0.3710	2.0434	0.3300	2.1674	0.2024
30	θ	1.0154	0.0686	1.0133	0.0640	1.0266	0.0626
	α	2.0316	0.1501	2.0228	0.1217	2.1105	0.1093
50	θ	1.0057	0.0394	1.0055	0.0374	1.0153	0.0355
	α	2.0098	0.0773	2.0165	0.0646	2.0620	0.0529
100	θ	1.0052	0.0192	1.0047	0.0175	1.0078	0.0155
	α	2.0020	0.0336	2.0107	0.0273	2.0328	0.0236
200	θ	1.0020	0.0086	1.0018	0.0078	1.0030	0.0070
	α	1.9992	0.0167	2.0060	0.0134	2.0153	0.0112
500	θ	1.0019	0.0036	1.0016	0.0032	1.0019	0.0028
	α	2.0000	0.0065	2.0027	0.0050	2.0059	0.0041
1000	θ	1.0023	0.0018	1.0020	0.0016	1.0015	0.0014
	α	2.0013	0.0033	2.0021	0.0025	2.0031	0.0020

6. Applications

This study utilizes two datasets: the first dataset represents the COVID-19 mortality rates of Italy recorded for a period of 111 days from 1 April to 20 July 2020, and the data can be found in [38]. The second dataset is survival times for 121 breast cancer patients treated over the period 1929–1938, quoted in [39].

The plot of COVID-19 data points in Figure 3(a) shows an extremely irregular and turbulent pattern characterized by several peaks and troughs spread out over time. Still, the data's erratic and varying characteristics can match trends seen in different COVID-19 metrics. The plot for the cancer dataset shown in Figure 3(b) appears to demonstrate an exponential growth trend or a strong positive correlation between the incidence or cases of two features over time.

The outcomes of fitting the EBSH and BSH distributions to two real-life data sets are compared in this section. As was covered in the previous part, we use the maximum likelihood to estimate the models' unknown parameters. R is used throughout all computations.

Table 15 presents the maximum likelihood estimates (MLEs) of the unknown parameters of the EBSH and BSH distributions for the COVID-19 data. We take into account the Akaike information criterion (AIC), consistent Akaike information criterion (CAIC), Bayesian information criterion (BIC), and Hannan-Quinn information criterion (HQIC) for the COVID-19 data to assess the distributions. These findings suggest that the EBSH distribution fits the COVID-19 data far better.

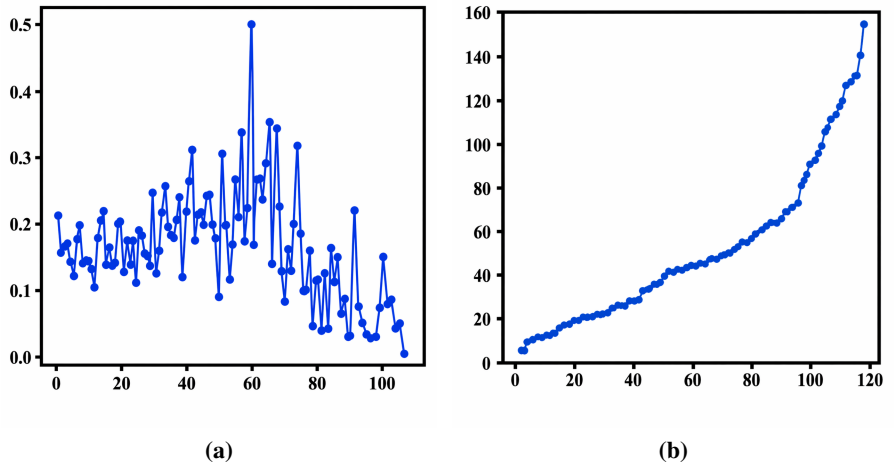

Figure 3. Plots of datasets.

Table 15. MLEs of the unknown parameters and the goodness-of-fit for the COVID-19 dataset.

Model	Parameter	AIC	CAIC	BIC	HQIC	LL
BSH	$\theta = 0.4421$	-21.5205	-21.4838	-18.811	-20.4213	11.7602
EBSH	$\theta = 0.0502$	-24.2351	-24.124	-18.816	-22.0367	14.1175
	$\alpha = 7.1557$					
BIII	$\beta = 1.1903$	-20.3428	-20.2317	-14.9238	-18.1445	12.1714
	$\gamma = 0.4142$					
IPCS	$\lambda = 0.6964$	-12.1325	-12.0213	-6.7134	-9.9341	8.0662
	$\mu = 1.2409$					
LogK	$a = 0.4696$	-21.7778	-21.6667	-16.3588	-19.5795	12.8889
	$b = 0.9474$					
Beta	$\pi = 0.4119$	-13.0020	-12.8909	-7.5830	-10.8037	8.5010
	$\psi = 0.6543$					
Weibull	$c = 0.9950$	21.5896	21.7007	27.0087	23.7880	-8.7948
	$d = 0.8114$					
LogG	$\sigma = 0.1808$	11.8533	11.9644	17.2723	14.0516	-3.9266
	$\tau = 7.7749$					

The MLEs of the unknown parameters of the EBSH and BSH distributions for the breast cancer data are shown in Table 16. To evaluate the distributions, we consider the AIC, CAIC, BIC, and HQIC for the breast cancer data. These results indicate that the EBSH distribution fits the data much better. Two real-world data sets were used to evaluate the statistical advantage of the EBSH distribution over its submodel (BSH) and other competing distributions, including Burr III (BIII) [40], inverse power chi-square (IPCS) [41], log-Kumaraswamy (LogK) [37], beta [42], Weibull [43], and log-gamma (LogG) models.

Table 16. MLEs of the unknown parameters and the goodness-of-fit for the cancer dataset.

Model	Parameter	AIC	CAIC	BIC	HQIC	LL
BSH	$\alpha = 0.3095$	-235.8310	-235.7970	-233.0350	-234.6950	118.9155
EBSH	$\theta = 0.0489$	-253.2060	-253.1040	-247.6140	-250.9350	128.6030
	$\alpha = 3.9910$					
BIII	$\beta = 0.5074$	-219.7791	-219.6774	-214.1875	-217.5081	111.8895
	$\gamma = 0.4508$					
IPCS	$\lambda = 0.2651$	-135.7348	-135.6331	-130.1433	-133.4639	69.8674
	$\mu = 0.6315$					
LogK	$a = 0.5243$	-207.5026	-207.4009	-201.9110	-205.2316	105.7513
	$b = 0.9028$					
Beta	$\pi = 0.1490$	-123.7110	-123.6093	-118.1194	-121.4400	63.8555
	$\psi = 0.1921$					
Weibull	$c = 0.8124$	-151.5817	-151.4800	-145.9901	-149.3107	77.7908
	$d = 0.2557$					
LogG	$\sigma = 0.1234$	-6.5092	-6.4075	-0.9176	-4.2382	5.2546
	$\tau = 7.6737$					

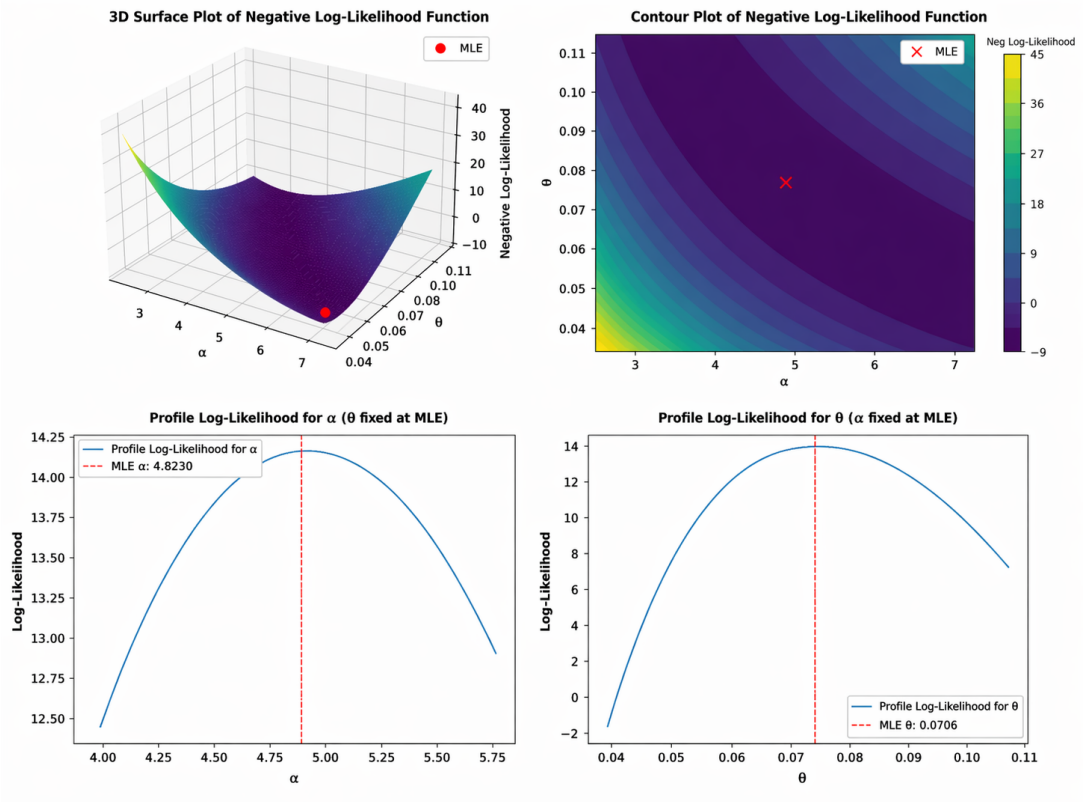

Figure 4. Likelihood and profile analysis for MLE estimation of the EBSH in COVID-19 dataset.

The robust statistical advantage demonstrated by the EBSH distribution in fitting both the complex, irregular COVID-19 mortality data and the trended breast cancer survival data, as shown by superior information criteria values, serves as a crucial foundation necessary for reliable and accurate subsequent comparative predictive modeling presented in the next section.

The likelihood surface for the COVID-19 dataset provided in Figure 4 is smooth and convex, with a unique global minimum, indicating that the maximum likelihood estimates are stable. The contour plot shows circular level curves, showing a considerable dependence between parameters. Profile likelihood analysis indicates that the α estimate is more precise, with a sharper peak, whereas θ has greater uncertainty due to a flatter profile. Therefore, the model is highly identifiable and provides reliable parameter estimates.

In the cancer dataset, the negative log-likelihood surface presented in Figure 5 has a smooth convex shape with a unique global minimum, indicating reliable parameter estimation. The contour plot exhibits circular level curves, indicating that the parameters are moderately dependent. Profile likelihood analysis shows that the estimate of α is more exact, with a sharper peak, whereas θ has greater uncertainty due to a flatter profile. Hence, the model shows good identifiability and reliable inference.

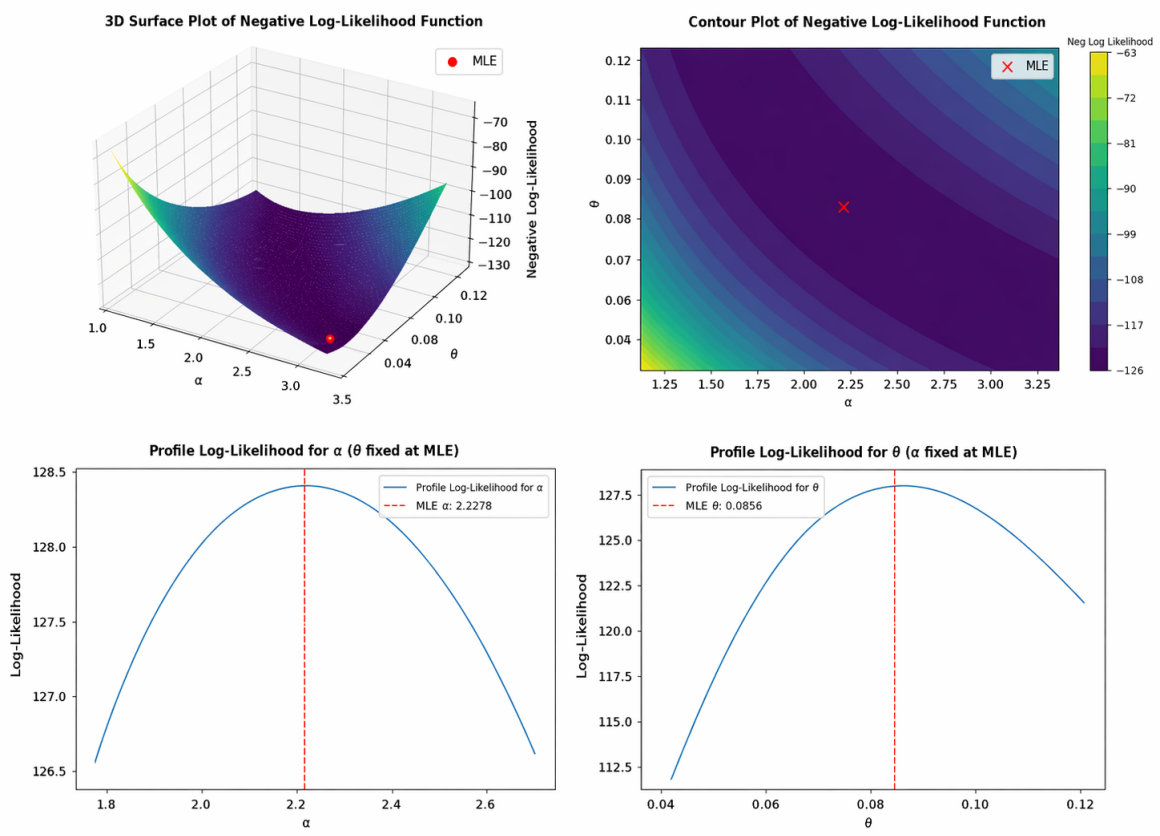

Figure 5. Likelihood and profile analysis for MLE estimation of the EBSH in the cancer dataset.

7. Prediction methodology

7.1. Data preprocessing

Machine learning requires preprocessing input data to construct an accurate prediction model. The datasets contain some missing values, which have been replaced using the mean value of each feature using the Pandas library in Python.

7.2. Data scaling

Features were scaled uniformly to improve the machine learning model's performance. The inclusion of a broader range of features can potentially dominate the model's objective function, leading to suboptimal performance. We employ min-max feature scaling to normalize all the data points across the datasets. Data scaling is also beneficial in mitigating the impact of outliers.

7.3. Prediction models

7.3.1. Recurrent neural network

An artificial neural network type called an RNN, known as a recurrent neural network, is made specifically to operate with sequence-containing time series data. Conventional neural network architecture lacks interlayer connections, which connect the input layer, hidden layer, and output layer. This limitation makes such neural networks insufficient for solving many problems [44]. RNNs are called so because the output of a sequence is influenced by its previous output. This means that the hidden layer nodes are not isolated but rather interconnected. The input to the hidden layer comprises both the production of the input layer and the previous hidden layer. An RNN has the idea of memory, which saves data from earlier inputs to produce the subsequent result [45]. RNNs differentiate themselves from typical neural networks through the utilization of parameter sharing. Equation (7.1) represents the output of a single neural network. The subsequent neuron receives the data x_{t-1}, $x_t, \ldots,$ which leads to the formation of the neural time series l_{t-1}, $l_t, \ldots,$

$$l_t = \sigma\left(w_t x_t + w_i x_{i-1} + d\right) \tag{7.1}$$

and

$$f\left(t\right) = \text{softmax}\left(w_y l_t + h\right), \tag{7.2}$$

Equation (7.1) represents the calculation of l_t using the activation function σ; the vector weights w_t, w_i; and bias value d. Equation (7.2) represents the calculation of the output $f(t)$ determined by vector weight w_y, calculated time series value l_t, and bias value h.

7.3.2. Support vector regression

Support vector regression (SVR) is a machine learning model used for regression analysis across various academic fields. The SVR model aims to reduce operational risk by identifying and defining an optimal margin around the data [46]. This is achieved by maximizing the distance between support vectors, which are the data points closest to the decision boundary. By maximizing this margin, SVR establishes a more robust solution, ensuring that the model generalizes well to unseen data. The objective of SVR is to discover the function y that best fits the training data x while maximizing the

margin between the support vectors. The function y is given in Eq (7.3), where ω denotes the weight vector, and d is a bias value.

$$y = f(x) = (\omega x + d). \tag{7.3}$$

7.3.3. Autoregressive integrated moving average

Autoregressive integrated moving average (ARIMA) is a statistical technique used to forecast future values in time series data. The Box-Jenkins methodology [47] provides a systematic approach for developing ARIMA models for univariate time series. This methodology involves creating a stationary time series by differencing the data (the "I" or integrated-d component) and then modeling the stationary series using a combination of autoregressive (AR) and moving average (MA) terms. The mathematical representation of the ARIMA model is expressed as follows:

$$Y_t = c_t + \sum_{i=1}^{p} \omega_m Y_{t-i} + \sum_{j=1}^{q} \theta_n e_{t-j}, \tag{7.4}$$

where Y_{t-i} is the lagged value at the time $t - i$, ω_m is the coefficient of the *mth* order of the AR model, Y_t is the predicted value, c_t is the constant value, and θ_n is the *nth* order of the MA model.

7.4. EBSH-based statistical feature engineering using CDF transformation

In this study, a statistical feature engineering approach based on the EBSH distribution is introduced to improve the predictive performance of ML models. Rather than using only raw observations as inputs to ML, the probabilistic structure of the data is incorporated by transforming them using the CDF of the EBSH distribution. This approach allows ML models to capture the underlying distributional characteristics of the data, including skewness, tail behavior, and distributional shape. Using the probability integral transform, each observation x_i is transformed into a probability value using the EBSH CDF as follows:

$$z_i = F(x_i). \tag{7.5}$$

This transformation maps the original data onto the probability space on the interval (0,1), thereby normalizing the data and embedding the statistical distribution's characteristics in the feature space. The transformed values obtained from the EBSH CDF were then used as input features for the ML models, specifically the RNN and SVR models.

7.4.1. Steps involved in the model training process with EBSH-based feature engineering

The overall procedure for model training using the EBSH-based statistical feature engineering approach is summarized in the following steps:

Step 1: Data collection

The dataset was obtained and arranged as a time series dataset for prediction modeling.

Step 2: Data scaling

A data scaling was applied to the original data to stabilize variance and reduce skewness in the dataset.

Step 3: Parameter estimation of the EBSH distribution

The parameters of the EBSH distribution were estimated using the maximum likelihood estimation method based on the transformed data.

Step 4: CDF transformation (statistical feature engineering)

The log-transformed data were transformed using the CDF of the EBSH distribution to obtain probability-based features.

Step 5: Feature construction

The transformed CDF values were used as input features for ML models. This process represents the statistical feature engineering stage.

Step 6: Train-test data split

The dataset was divided into training and testing sets using a 90:10 split to evaluate predictive performance.

Step 7: Model training

The ML models (RNN and SVR) were trained using the transformed features obtained from the EBSH CDF.

Step 8: Model prediction

The trained models were used to generate predictions on the testing dataset.

Step 9: Performance evaluation

Model performance was evaluated using several performance metrics, including MAE, RMSE, MAPE, and MPE.

Step 10: Comparative analysis

The predictive performance of models trained using the original data and the EBSH-transformed features was compared to evaluate the effectiveness of the proposed statistical feature engineering approach.

7.4.2. Summary of the proposed method

The overall predictive modelling used in this study can be summarized as follows:

$$OriginalData \rightarrow F_{EBSH(x)} \rightarrow FeatureEngineering \rightarrow ML(RNN/SVR) \rightarrow Prediction.$$

This method represents a hybrid statistical ML approach in which the EBSH distribution is used as a statistical feature engineering tool to enhance ML prediction performance.

7.5. Empirical results and analysis

This section presents the results of the performance of the predictive model. The datasets were split into two sets: a training set, which comprised 90% of the data, and a test set, which comprised 10% of the data.

7.5.1. Grid search hyperparameter tuning

The grid search approach is an independent search algorithm that systematically evaluates all potential combinations of hyperparameters within the search space to determine the combination that yields the best performance [48]. The technique is exploratory and evaluates the performance of hyperparameters at every possible setting, making it an exhaustive search approach. Best hyperparameters were determined for SVR and RNN using a grid search approach.

7.6. Prediction error

The methods used for estimating errors involve error rates and percentage errors. The error rates of mean absolute error (MAE) and root mean square error (RMSE) were used [49]. MAE calculates the absolute difference between the values that were predicted and actual values, and RMSE provides a measure of the standard deviation of those errors. Additionally, we use the mean absolute percentage error (MAPE) and mean percentage error (MPE) to assess relative errors. MAPE calculates the average percentage difference between predicted and actual values, providing an intuitive understanding of the model's accuracy. MPE, on the other hand, evaluates the mean percentage difference between the predicted and actual values. The mathematical expressions are given in Eqs (7.6)–(7.9).

$$MAE = \frac{1}{n}\sum_{i=1}^{n}(|x_i - y_i|), \tag{7.6}$$

$$MAPE = \frac{1}{n}\sum_{i=1}^{n}\left(\frac{|x_i - y_i|}{x_i}\right), \tag{7.7}$$

$$MPE = \frac{1}{n}\sum_{i=1}^{n}\left(\frac{x_i - y_i}{x_i}\right), \tag{7.8}$$

and

$$RMSE = \sqrt{\frac{1}{n}\sum_{i=1}^{n}(x_i - y_i)^2}, \tag{7.9}$$

where n is the number of observations, x_i is the actual value, and y_i is the predicted value.

7.7. COVID-19 dataset

The hyperparameter ranges are summarized in Table 17. The input data were formatted as sequences with a look-back length of 6 and a single feature. A four-layer sequential model with ReLU activation functions was employed for forecasting. The model consists of dense (fully connected) layers, culminating in a single output unit to generate predictions. The Adam optimizer was used to minimize the mean squared error loss function during training. The training was conducted using a batch size of 4, a learning rate of 0.001, and 120 epochs.

Table 17. RNN hyperparameters for the COVID-19 dataset.

Hyperparameter	Value
Learning rate	0.001
Number of epochs	120
Batch size	4
Activation function	ReLu
Optimizer	Adam

Table 18 details the SVR training hyperparameters. The regularization parameter, denoted as C, was set to 1, and the kernel function employed was the radial basis function (RBF) with a gamma

value of 0.01. The gamma parameter controls the influence of individual data points on the decision boundary in the RBF kernel.

Table 18. SVR hyperparameters for the COVID-19 dataset.

Hyperparameter	Value
C	1
Gamma	0.01
Kernel function	RBF

7.7.1. Results of ML training before feature engineering

From Table 19, the RNN appears to outperform other models. The SVR model demonstrated the weakest performance among the two competing ML models, exhibiting the highest error values across all metrics.

Table 19. Prediction errors for the COVID-19 dataset before feature engineering.

Metric	RNN	SVR
MAE	0.0296	0.1208
MAPE	0.3804	3.0634
MPE	0.1526	3.0633
RMSE	0.0373	0.1257

In Figure 6, the RNN model demonstrates successful convergence, as the validation loss (orange line) closely aligns with the training loss (blue line). This indicates that the model has learned the underlying patterns of the training data without overfitting, achieving good generalization to unseen data.

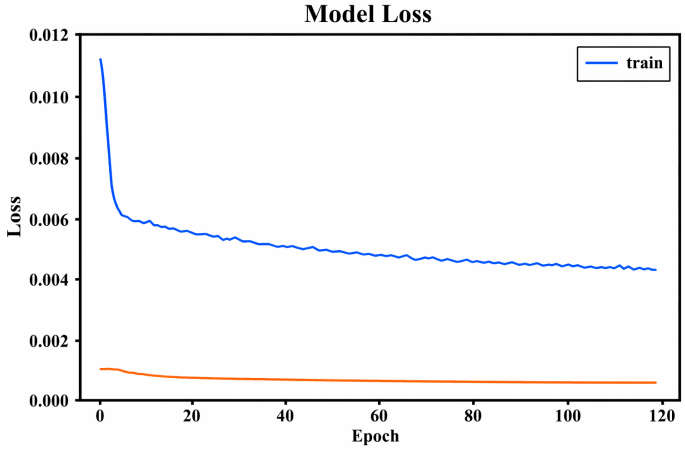

Figure 6. Training loss for RNN for the COVID-19 dataset before feature engineering.

7.7.2. Results of ML training after feature engineering

The results for the COVID-19 dataset presented in Table 20 indicate that the RNN model outperforms the SVR model across all evaluation metrics after applying the EBSH-based statistical feature engineering transformation. The RNN achieved lower MAE, MAPE, and RMSE values, indicating higher prediction accuracy and better model fit compared to SVR. The positive MPE values for both models suggest a slight underestimation bias, although the bias is smaller for the RNN model. Overall, the results suggest that the probabilistic features generated from the EBSH CDF transformation improve model learning, particularly for the RNN model, which is better suited for sequential and nonlinear data patterns.

Table 20. Prediction errors for the COVID-19 dataset after feature engineering.

Metric	RNN	SVR
MAE	0.1039	0.1172
MAPE	0.1246	0.1388
MPE	0.0379	0.0531
RMSE	0.1291	0.1410

The training error plots in Figure 7 show that both RNN and SVR models can capture the overall trend of the COVID-19 dataset; however, the RNN model follows the actual observations more closely, indicating better learning of nonlinear temporal patterns, whereas the SVR model produces smoother predictions, indicating stronger generalization but lower flexibility.

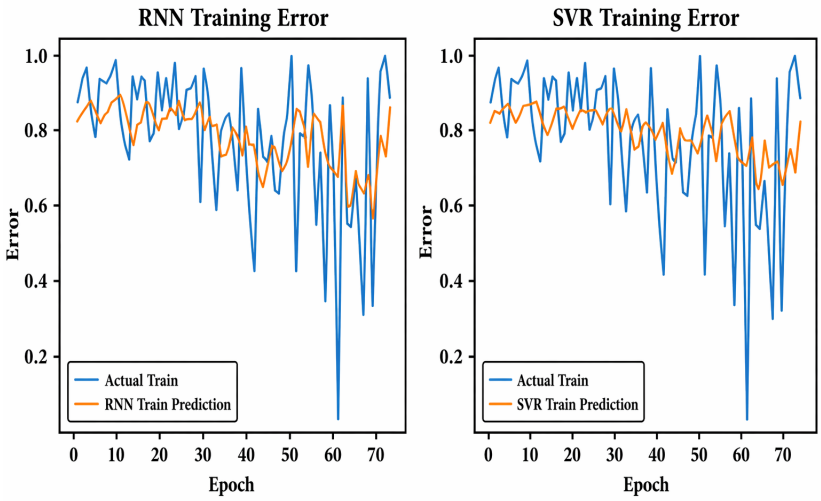

Figure 7. Training errors for RNN and SVR of the COVID-19 dataset after feature engineering.

7.8. Cancer dataset

The hyperparameters used for RNN are presented in Table 21. The sequential model consists of six hidden layers with ReLU activation functions, receiving input data formatted as sequences with a specified look-back length of 6 and a single feature. The final layer is a dense (fully connected) layer with a single output unit for predictions. The model was compiled using the Adam optimizer with a learning rate of 0.001 and a mean squared error (MSE) loss function. Training was performed for 120 epochs with a batch size of 4. Additionally, the regularization parameter C was set to 1000 to prevent overfitting.

Table 21. RNN hyperparameters for the cancer dataset.

Hyperparameter	Value
Learning rate	0.001
Number of epochs	120
Batch size	4
Activation function	ReLu
Optimizer	Adam

The hyperparameters used for SVR are summarized in Table 22. The radial basis function (RBF) kernel was employed, with a gamma value of 0.001. In the RBF kernel, gamma determines the influence of individual data points on the decision boundary: a smaller gamma value, like 0.001, indicates a broader area of influence for each data point.

Table 22. SVR hyperparameters for the cancer dataset.

Hyperparameter	Value
C	1000
Gamma	0.001
Kernel function	RBF

As shown in Table 23, SVR is the best-performing model with the lowest prediction errors, with an MAE of 4.0177, MAPE of 0.0316, MPE of 0.0163, and RMSE of 4.9926. The RNN has the lowest percentage of errors with an MAPE of 0.053 and MPE of 0.0027; it also has the largest error rates with an MAE of 6.8835 and RMSE of 7.9822. In conclusion, the SVR model seems to be the most effective prediction model according to the evaluations given. Although the RNN model outperforms other models in terms of percentage mistakes, it results in the most overall errors.

Table 23. Prediction errors for the cancer dataset before feature engineering.

Metric	RNN	SVR
MAE	6.8835	4.0177
MAPE	0.053	0.0316
MPE	0.0027	0.0163
RMSE	7.9822	4.9926

The plot in Figure 8 represents the training loss of the RNN model for the cancer dataset. The model has effectively memorized the patterns in the training data but cannot adapt to new data. The plot in Figure 9 shows the training error of SVR for the cancer dataset. The predictions on the training set (orange curve) closely match the actual values, demonstrating the model's ability to fit the training data well. Although the predictions on the test set (green curve) do not perfectly align with the actual values (light blue curve), they can capture the underlying trend, indicating the model's capacity to generalize beyond the training samples.

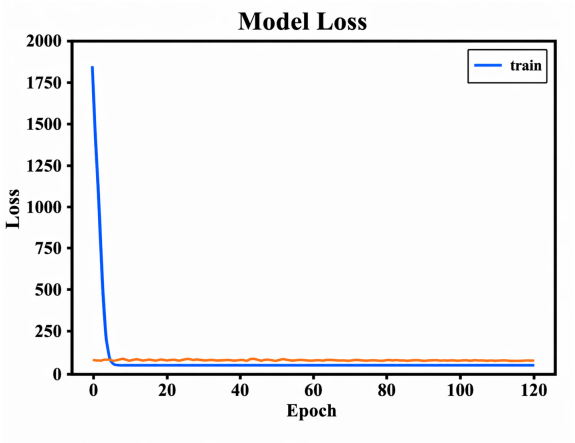

Figure 8. Training loss for the RNN of the cancer dataset before feature engineering.

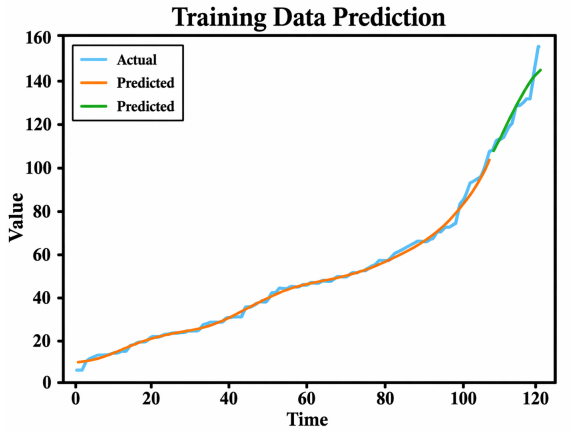

Figure 9. SVR training error plot for cancer dataset before feature engineering.

7.8.1. Results of ML training after feature engineering

For the cancer dataset presented in Table 24 , the RNN model produced extremely small error values across all performance metrics, indicating very high prediction accuracy after applying the EBSH-based statistical feature engineering transformation. The MAE, MAPE, and RMSE values are close to zero, suggesting that the predicted values closely match the actual values. The MPE value is slightly negative, indicating a negligible overestimation bias. In contrast, the SVR model shows higher error values, indicating that it does not benefit from the EBSH feature transformation as much as the RNN model. This result suggests that deep learning models may better utilize distribution-based engineered features than traditional machine learning models.

Table 24. Prediction errors for the cancer dataset after feature engineering.

Metric	RNN	SVR
MAE	0.0002	0.1000
MAPE	0.0002	0.0990
MPE	-0.0002	0.0990
RMSE	0.0002	0.1000

The training plots for the cancer dataset in Figure 10 show that the RNN model closely fits the training data, indicating strong learning capability, whereas the SVR model captures only the general trend and appears to underfit the data. This explains the superior predictive performance of the RNN model after applying the EBSH-based statistical feature engineering transformation.

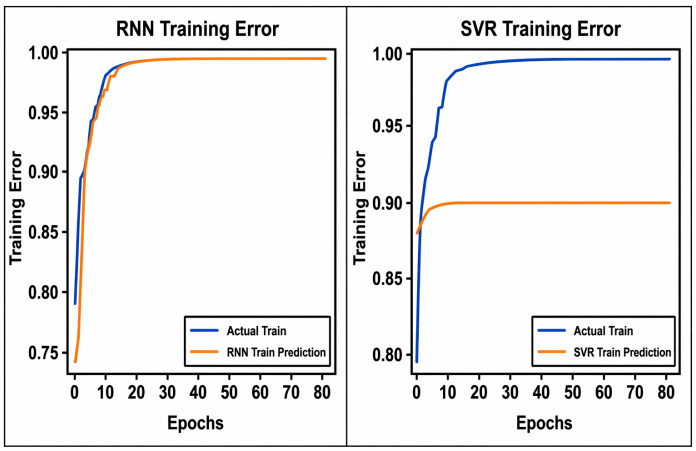

Figure 10. Training errors for RNN and SVR of cancer dataset after feature engineering.

The SVR model underperformed relative to the RNN model because kernel-based regression methods are less flexible in capturing complex nonlinear temporal dependencies, whereas recurrent neural networks can learn sequential patterns and adapt to distribution-transformed features more effectively.

The results demonstrate that the EBSH-based statistical feature engineering approach improves predictive performance for both datasets by incorporating distributional information into the ML

models. The transformation using the EBSH CDF helps capture the underlying statistical structure of the data, leading to improved prediction accuracy. Across both datasets, the RNN model consistently outperforms the SVR model, indicating that combining statistical feature engineering with deep learning models provides a more effective predictive model than traditional ML approaches.

7.9. Results and discussions

The comparison between the raw ML results and the EBSH feature engineering results for the COVID-19 dataset shows that the RNN model remains the best-performing model in both cases, whereas the SVR model continues to have higher prediction errors. However, after applying the EBSH-based statistical feature engineering transformation, the percentage error measures (MAPE and MPE) are significantly reduced for both RNN and SVR, indicating improved relative prediction accuracy and model stability. Although the absolute error measures (MAE and RMSE) change slightly after transformation, the EBSH transformation helps normalize the data and improve the learning structure of the models, particularly in terms of percentage error performance.

For the cancer dataset, the raw ML results show that the SVR model performs better than the RNN model in terms of MAE and RMSE, whereas the RNN model performs better in percentage error metrics. After applying the EBSH feature engineering transformation, the RNN model shows a very large improvement in prediction accuracy, with extremely small error values across all metrics, whereas the SVR model also shows improved performance but not as significantly as the RNN model. This indicates that the EBSH-based feature engineering transformation is particularly effective for the cancer dataset, especially for the RNN model.

The comparative analysis before and after EBSH feature engineering demonstrates that incorporating the EBSH distribution through statistical feature engineering improves the predictive performance of ML models. The transformation helps incorporate distributional information, stabilize the data, and improve model learning. Across both datasets, the RNN model benefits more from the EBSH feature engineering than the SVR model, indicating that deep learning models may better utilize probabilistic feature transformations. These results confirm that the EBSH-based statistical feature engineering framework provides a more robust predictive modeling approach compared to using raw data alone.

The results demonstrate that the proposed EBSH-based statistical feature engineering approach improves ML prediction performance by incorporating distributional information into the feature space, thereby enhancing model learning capability and reducing prediction errors, particularly for deep learning models such as RNN.

The results show that the use of EBSH-based statistical feature engineering improves the predictive performance of the ML models for both the COVID-19 and cancer datasets. By transforming the data using the EBSH cumulative distribution function, the original observations are converted into probability-based features that better reflect the underlying distributional structure of the data. This transformation helps stabilize the data, reduce the effect of extreme values, and improve the overall learning process of the models.

The improvement in performance was more noticeable for the RNN model than for the SVR model. This is likely because the RNN model is designed to capture nonlinear patterns and sequential relationships in the data, allowing it to benefit more from the transformed probabilistic features. The SVR model, on the other hand, relies on kernel-based regression and may not fully capture complex

temporal patterns, which explains its relatively lower performance after transformation.

The results suggest that combining statistical distribution-based feature engineering with ML models provides a more effective predictive modeling approach than using raw data alone. The EBSH-based feature engineering approach therefore improves prediction accuracy by incorporating statistical information into the machine learning modeling process.

Note that the EBSH distribution is not used as a standalone predictive model; rather, it is used as a statistical feature engineering tool to transform the data before applying machine learning prediction models, thereby ensuring a fair comparative predictive framework.

8. Conclusions

The EBSH distribution was presented in this paper. The EBSH model was constructed using a transformation approach to expand the existing BSH model. An explicit version of the distribution, density, survival, and hazard functions was provided. The EBSH distribution might be symmetric, right-skewed, rising, decreasing, or bathtub-shaped. The moments, the moment-generating function, the quantile function, and other fundamental statistical properties were investigated and derived. A maximum-likelihood estimation method was used to estimate the model's parameters. A simulation analysis was carried out using randomly generated samples of different sizes to determine the failure rate and the form of the PDF computationally. This study employed a dual methodology to validate the model and its utility. First, numerical analysis on COVID-19 death rates and breast cancer data demonstrated that the EBSH distribution provides superior statistical fits compared to the alternative BSH model, as verified by lower AIC, BIC, and other information criteria. Second, we performed a comparative predictive analysis using AI and time series models (RNN, SVR, ARIMA, and exponential smoothing) on these same complex medical datasets. The predictive results confirmed that the RNN achieved the lowest error metrics (MAE of 0.0296, RMSE of 0.0373) and outperformed other models when forecasting COVID-19 mortality data. Conversely, the SVR model demonstrated the best performance for forecasting the breast cancer survival times, yielding the lowest MAE (4.0177) and RMSE (4.9926). We anticipate that the suggested distribution will have a larger audience and serve as an essential tool for simulating a variety of events across numerous fields. The proposed EBSH distribution contributes to the growing class of flexible statistical models by bridging the gap between theoretical tractability and practical applicability. Its ability to accommodate diverse hazard rate structures and varying skewness patterns makes it particularly valuable in reliability engineering, survival analysis, and medical data modeling.

Future study will look into different estimation techniques, such as Bayesian, to improve the proposed model. Using a variety of datasets from different fields not discussed in this paper, the utility of the EBSH distribution will be assessed. Additionally, the bivariate forms of the EBSH distribution will be the primary concern of the subsequent approach.

Author contributions

Abdulrahman M. A. Aldawsari: Formal analysis, Writing–review and editing; Zahrah Fayez Althobaiti: Validation, Investigation, Supervision, Writing–review and editing, Data curation, Methodology; Aminu Suleiman Mohammed: Conceptualization, Writing–review and editing,

Software, Investigation, Methodology; Abdulmajeed A. R. Alharbi: Formal analysis, Writing original draft, Investigation, Resources, Funding. All authors have read and agreed to the published version of the manuscript.

Use of Generative-AI tools declaration

The authors declare they have not used Artificial Intelligence (AI) tools in the creation of this paper.

Acknowledgments

This study is supported via funding from Prince sattam bin Abdulaziz University project number (PSAU/2026/R/1447).

Conflict of interest

The authors declare no conflicts of interest in this paper.

References

1. H. J. Wang, J. R. Zhang, B. Li, F. Z. Xuan, Machine learning-based fatigue life prediction of laser powder bed fusion additively manufactured Hastelloy X via nondestructively detected defects, *Int. J. Struct. Integr.*, **16** (2025), 104–126. https://doi.org/10.1108/IJSI-09-2024-0161
2. L. W. Dang, X. F. He, D. C. Tang, H. Xin, B. Wu, A fatigue life prediction framework of laser-directed energy deposition Ti-6Al-4V based on physics-informed neural network, *Int. J. Struct. Integr.*, **16** (2025), 327–354. https://doi.org/10.1108/IJSI-10-2024-0170
3. S. Y. Yang, D. B. Meng, H. T. Wang, C. Yang, A novel learning function for adaptive surrogate-model-based reliability evaluation, *Philos. Trans. A Math. Phys. Eng. Sci.*, **382** (2024), 20220395. https://doi.org/10.1098/rsta.2022.0395
4. H. Daud, A. A. Suleiman, A. I. Ishaq, N. Alsadat, M. Elgarhy, A. Usman, et al., A new extension of the Gumbel distribution with biomedical data analysis, *J. Radiat. Res. Appl. Sci.*, **17** (2024), 101055. https://doi.org/10.1016/j.jrras.2024.101055
5. N. G. Nia, E. Kaplanoglu, A. Nasab, Evaluation of artificial intelligence techniques in disease diagnosis and prediction, *Discover Artif. Intell.*, **3** (2023), 5. https://doi.org/10.1007/s44163-023-00049-5
6. B. Saravi, F. Hassel, S. Ülkümen, A. Zink, V. Shavlokhova, S. Couillard-Despres, et al., Artificial intelligence-driven prediction modeling and decision making in spine surgery using hybrid machine learning models, *J. Pers. Med.*, **12** (2022), 509. https://doi.org/10.3390/jpm12040509
7. M. A. Ghorbani, R. Khatibi, V. Karimi, Z. M. Yaseen, M. Zounemat-Kermani, Learning from multiple models using artificial intelligence to improve model prediction accuracy: application to river flows, *Water Resour. Manag.*, **32** (2018), 4201–4215. https://doi.org/10.1007/s11269-018-2038-x

8. S. G. Nia, Appropriate combination of artificial intelligence and algorithms for increasing predictive accuracy management, *J. Inf. Technol. Manag.*, **2** (2010), 157–174.
9. N. Alotaibi, A. S. Al-Moisheer, A. S. Hassan, I. Elbatal, S. A. Alyami, E. M. Almetwally, Epidemiological modeling of COVID-19 data with advanced statistical inference based on Type-II progressive censoring, *Heliyon*, **10** (2024), e36774. https://doi.org/10.1016/j.heliyon.2024.e36774
10. T. Hirayama, Epidemiology of breast cancer with special reference to the role of diet, *Preventive Med.*, **7** (1978), 173–195. https://doi.org/10.1016/0091-7435(78)90244-X
11. A. A. Suleiman, H. Daud, A. I. Ishaq, A. U. Farouk, A. S. Mohammed, M. Kayid, et al., A new statistical model for advanced modeling of cancer disease data, *Kuwait J. Sci.*, **52** (2025), 100429. https://doi.org/10.1016/j.kjs.2025.100429
12. S. Ferrari, F. Cribari-Neto, Beta regression for modelling rates and proportions, *J. Appl. Stat.*, **31** (2004), 799–815. https://doi.org/10.1080/0266476042000214501
13. R. Kieschnick, B. D. McCullough, Regression analysis of variates observed on (0,1): percentages, proportions and fractions, *Stat. Model.*, **3** (2003), 193–213. https://doi.org/10.1191/1471082X03st053oa
14. M. C. Korkmaz, A new heavy-tailed distribution defined on the bounded interval: the logit slash distribution and its application, *J. Appl. Stat.*, **47** (2020), 2097–2119. https://doi.org/10.1080/02664763.2019.1704701
15. J. R. van Dorp, S. Kotz, The standard two-sided power distribution and its properties: with applications in financial engineering, *Amer. Statist.*, **56** (2002), 90–99. https://doi.org/10.1198/000313002317572745
16. N. L. Johnson, Systems of frequency curves generated by methods of translation, *Biometrika*, **36** (1949), 149–176. https://doi.org/10.2307/2332539
17. C. W. Topp, F. C. Leone, A family of J-shaped frequency functions, *J. Amer. Statist. Assoc.*, **50** (1955), 209–219. https://doi.org/10.1080/01621459.1955.10501259
18. A. Pourdarvish, S. M. T. K. Mirmostafaee, K. Naderi, The exponentiated Topp-Leone distribution: properties and application, *J. Appl. Environ. Biol. Sci.*, **5** (2015), 251–256.
19. A. Fayomi, A. S. Hassan, E. M. Almetwally, Inference and quantile regression for the unit-exponentiated Lomax distribution, *PLoS One*, **18** (2023), e0288635. https://doi.org/10.1371/journal.pone.0288635
20. M. C. Korkmaz, C. Chesneau, On the unit Burr-XII distribution with the quantile regression modeling and applications, *Comput. Appl. Math.*, **40** (2021), 29. https://doi.org/10.1007/s40314-021-01418-5
21. R. A. R. Bantan, F. Jamal, C. Chesneau, M. Elgarhy, Theory and applications of the unit Gamma/Gompertz distribution, *Mathematics*, **9** (2021), 1850. https://doi.org/10.3390/math9161850
22. A. S. Hassan, A. Fayomi, A. Algarni, E. M. Almetwally, Bayesian and non-Bayesian inference for unit-exponentiated half-logistic distribution with data analysis, *Appl. Sci.*, **12** (2022), 11253. https://doi.org/10.3390/app122111253

23. A. S. Mohammed, F. I. Ugwuowo, On transmuted exponential-Topp Leone distribution with monotonic and non-monotonic hazard rates and its applications, *Reliab. Theory Appl.*, **16** (2021), 197–209.
24. A. S. Hassan, A. M. Khalil, H. F. Nagy, Data analysis and classical estimation methods of the bounded power Lomax distribution, *Reliab. Theory Appl.*, **19** (2024), 770–789.
25. A. S. Hassan, R. S. Alharbi, Different estimation methods for the unit inverse exponentiated Weibull distribution, *Commun. Stat. Appl. Methods*, **30** (2023), 191–213.
26. A. Saeed, A. Saboor, F. Jamal, N. Alsadat, O. S. Balogun, A. Faal, et al., Bounded sine hyperbolic distribution with applications to real datasets, *Kuwait J. Sci.*, **52** (2025), 100467. https://doi.org/10.1016/j.kjs.2025.100467
27. R. C. Gupta, P. L. Gupta, R. D. Gupta, Modeling failure time data by Lehmann alternatives, *Comm. Statist. Theory Methods*, **27** (1998), 887–904. https://doi.org/10.1080/03610929808832134
28. N. Eugene, C. Lee, F. Famoye, Beta-normal distribution and its applications, *Comm. Statist. Theory Methods*, **31** (2002), 497–512. https://doi.org/10.1081/STA-120003130
29. G. M. Cordeiro, M. de Castro, A new family of generalized distributions, *J. Stat. Comput. Simul.*, **81** (2011), 883–898. https://doi.org/10.1080/00949650903530745
30. I. A. Elbatal, T. S. Helal, A. M. Elsehetry, R. S. Elshaarawy, Topp-Leone Weibull generated family of distributions with applications, *J. Bus. Environ. Sci.*, **1** (2022), 183–195.
31. G. R. Al-Dayian, A. El-Helbawy, F. Abd El-Maksoud, Bayesian and maximum likelihood estimation for mixture models of the new Topp-Leone-G family, *J. Bus. Environ. Sci.*, **4** (2025), 210–253.
32. D. Soliman, M. A. Hegazy, G. R. Al-Dayian, A. A. El-Helbawy, Statistical properties and applications of a new truncated Zubair-generalized family of distributions, *Comput. J. Math. Stat. Sci.*, **4** (2025), 222–257.
33. A. Alzaatreh, C. Lee, F. Famoye, A new method for generating families of continuous distributions, *Metron*, **71** (2013), 63–79. https://doi.org/10.1007/s40300-013-0007-y
34. A. Yahaya, A. S. Mohammed, Transmuted Kumaraswamy-inverse exponential distribution: its properties and applications, *Niger. J. Sci. Res.*, **16** (2017), 298–307.
35. M. C. Jones, Families of distributions arising from distributions of order statistics, *Test*, **13** (2004), 1–43. https://doi.org/10.1007/BF02602999
36. M. Garg, On generalized order statistics from Kumaraswamy distribution, *Tamsui Oxf. J. Math. Sci. (TOJMS)*, **25** (2009), 153–166.
37. A. I. Ishaq, A. A. Suleiman, H. Daud, N. S. S. Singh, M. Othman, R. Sokkalingam, et al., Log-Kumaraswamy distribution: its features and applications, *Front. Appl. Math. Stat.*, **9** (2023), 1258961. https://doi.org/10.3389/fams.2023.1258961
38. A. S. Hassan, E. M. Almetwally, G. M. Ibrahim, Kumaraswamy inverted Topp-Leone distribution with applications to COVID-19 data, *Comput. Mater. Continua*, **68** (2021), 337–358. https://doi.org/10.32604/cmc.2021.013971
39. J. W. Boag, Maximum likelihood estimates of the proportion of patients cured by cancer therapy, *J. R. Stat. Soc. Ser. B*, **11** (1949), 15–53.

40. I. W. Burr, Cumulative frequency functions, *Ann. Math. Stat.*, **13** (1942), 215–232.

41. A. I. Ishaq, A. A. Abiodun, A. A. Suleiman, A. Usman, A. S. Mohammed, M. Tasiu, Modelling Nigerian inflation rates from January 2003 to June 2023 using newly developed inverse power chi-square distribution, In: *2023 4th International Conference on Data Analytics for Business and Industry (ICDABI)*, Bahrain, 2023, 644–651. https://doi.org/10.1109/ICDABI60145.2023.10629442

42. N. L. Johnson, S. Kotz, N. Balakrishnan, Beta distributions, In: *Continuous univariate distributions*, 2 Eds., John Wiley and Sons, 1994, 221–235.

43. W. Weibull, A statistical distribution function of wide applicability, *J. Appl. Mech.*, **18** (1951), 293.

44. P. Kumari, V. Goswami, H. Narasimhamurthy, R. S. Pundir, Recurrent neural network architecture for forecasting banana prices in Gujarat, India, *PLoS One*, **18** (2023), e0275702. https://doi.org/10.1371/journal.pone.0275702

45. T. Wilberforce, A. Alaswad, A. Garcia-Perez, Y. C. Xu, X. H. Ma, C. Panchev, Remaining useful life prediction for proton exchange membrane fuel cells using combined convolutional neural network and recurrent neural network, *Int. J. Hydrogen Energy*, **48** (2023), 291–303. https://doi.org/10.1016/j.ijhydene.2022.09.207

46. W. Cai, X. D. Wen, C. E. Li, J. J. Shao, J. G. Xu, Predicting the energy consumption in buildings using the optimized support vector regression model, *Energy*, **273** (2023), 127188. https://doi.org/10.1016/j.energy.2023.127188

47. S. Makridakis, M. Hibon, ARMA models and the Box-Jenkins methodology, *J. Forecast.*, **16** (1997), 147–163.

48. M. Ogunsanya, J. Isichei, S. Desai, Grid search hyperparameter tuning in additive manufacturing processes, *Manufactur. Lett.*, **35** (2023), 1031–1042. https://doi.org/10.1016/j.mfglet.2023.08.056

49. F. Kuran, G. Tanırcan, E. Pashaei, Performance evaluation of machine learning techniques in predicting cumulative absolute velocity, *Soil Dyn. Earthq. Eng.*, **174** (2023), 108175. https://doi.org/10.1016/j.soildyn.2023.108175

AIMS Press